Available online at www.sciencedirect.com
ScienceDirect
Precambrian Research 151 (2006) 31–52
Precambrian Research
www.elsevier.com/locate/precamres

Late Neoproterozoic Dokhan Volcanics, North Eastern Desert, Egypt: Geochemistry and petrogenesis

H.A. Eliwa [a,*], J.-I. Kimura [b], T. Itaya [c]

[a] *Geology Department, Faculty of Science, Minufiya University, Egypt*
[b] *Department of Geoscience, Faculty of Science & Engineering, Shimane University, Japan*
[c] *Research Institute of Natural Sciences, Okayama University of Science, 1-1 Ridai-cho, Okayama 700, Japan*

Received 15 September 2005; received in revised form 1 August 2006; accepted 15 August 2006

Abstract

Origin and tectonic setting of the late Neoproterozoic Dokhan Volcanics (ca. 610–560 Ma by whole rock Rb–Sr and ca. 600–590 Ma by SHRIMP U–Pb zircon) in the Egyptian Eastern Desert is debated. Debate concerns the tectonic setting they formed in, during transition between convergent to extensional, during or after collision of E and W Gondwana ~600 Ma. In order to solve this problem, we studied the geology and analyzed major and trace elements of lavas from Wadi Um Sidra and Um Asmer in the northern Eastern Desert. These range from medium- to high-K basalt to rhyolite. They comprise voluminous medium- to high-K calc-alkaline lavas, subordinate adakitic lavas, and minor alkali basalt. Adakitic lavas contain very low Y (<18 ppm) and heavy REE (HREE) (Yb ≤ 1 ppm) contents, with high Sr (>767 ppm) and Sr/Y (>40). They also have high Cr and Ni and low Nb, Rb, and Zr contents compared to coexisting calc-alkaline lavas. The adakitic lavas exhibit a fractionated rare earth element (REE) patterns with HREE depletion (La_N/Lu_N = 11.1–14.4), while calc-alkaline rocks have less fractionated REE patterns (La_N/Lu_N = 6.3–9.4). REE patterns of the alkali basalt are also similar to that of adakitic lavas. These alkali basalt, calc-alkaline, and adakitic lavas all show enrichment in large ion lithophile elements (LILEs) and show negative Nb–Ta anomalies with high Th/Zr, which suggest involvement of subducted slab melts in their petrogenesis. Our proposal is subduction of hot oceanic ridge before collision and later melting of the hot oceanic slab beneath Dokhan even after collision event.

Keywords: Dokhan Volcanics; Calc-alkaline; Adakite; Alkali basalt; Neoproterozoic; Egypt

1. Introduction

Egyptian basement rocks in the Eastern Desert and Sinai comprise Neoproterozoic juvenile crust developed in the northwestern-most Arabian–Nubian Shield (ANS; Stern, 2002). This crust includes dismembered ophiolites, volcano-sedimentary successions, and calc-alkaline I-type intrusive complexes. Most previous geological studies (Vail, 1985; Bentor, 1985; El Gaby et al., 1988; Kröner et al., 1988; Stern, 1994) reveal an essential role of convergent processes in the evolution of the Egyptian basement complex. The processes include (1) subduction, (2) accretion of intra-oceanic island arcs, back arc basins, and micro-continental plates, followed by (3) crustal thickening (Stern, 1994). These processes took place during Neoproterozoic time between about 900 and 614 Ma (Stern and Hedge, 1985; Kröner et al., 1992; Beyth et al., 1994; Stern, 1994). The terminal stage (614–550 Ma) of crustal evolution is characterized by (1) the eruption of the Dokhan Volcanics (El Ramly, 1972; Stern and Hedge, 1985), (2) deposition of molasse-type Hammamat sediments (Grothaus et al., 1979; Akaad

* Corresponding author. Tel.: +20 4823 27268; fax: +20 4823 5679.
E-mail address: eliwa98@yahoo.com (H.A. Eliwa).

0301-9268/$ – see front matter © 2006 Elsevier B.V. All rights reserved.
doi:10.1016/j.precamres.2006.08.005

and Noweir, 1980), and (3) shallow emplacement of the Younger Granites (El Gaby, 1975). Many studies have been carried out on the petrography and geochemistry of the Dokhan Volcanics (Basta et al., 1980; Stern and Gottfried, 1986; El Gaby et al., 1988, 1989; Abdel Rahman, 1996; Mohammed et al., 2000; Eliwa, 2000; Moghazi, 2003; El Sayed et al., 2004). These show that the Dokhan Volcanics have medium- to high-K calc-alkaline affinities. There is consensus that fractional crystallization of basaltic magma coupled with minor crustal contamination controlled the magmatic evolution. However, interpretations of tectonic setting are still controversial, especially whether they have been formed (1) in a subduction environment (Hassan and Hashad, 1990; El Gaby et al., 1988, 1990; Abdel Rahman, 1996), (2) in association with extension after crustal thickening (Stern et al., 1984, 1988; Stern, 1994; Fritz et al., 1996), or (3) during transition between subduction and extension (Ressetar and Monard, 1983; Mohammed et al., 2000).

Here we contribute to this discussion by providing new geological and geochemical data on Dokhan lavas exposed just north of the type locality at Gebel Dokhan (Fig. 1a), in order to better understand their origin and tectonic setting. Moreover, these data provide an excellent opportunity to understand source component(s) and processes involved in magma genesis and evolution.

2. Geological setting

2.1. Regional geology

Three groups of Neoproterozoic volcanic rocks have been identified in the basement complex of Egypt. The oldest two groups are known as the Older Metavolcanics (OMV) and Younger Metavolcanics (YMV) (Stern, 1981) and largely occur in the central and southern Eastern Desert. These volcanics are mainly mafic to intermediate with subordinate felsic rocks. OMV are low-K tholeiitic and YMV are low- to medium-K calc-alkaline, and are the products of subduction-related processes (back-arc basins and island arcs). The third group (ca. 610–560 Ma), known as Dokhan Volcanics, is restricted mainly in the North Eastern Desert and southern Sinai (Moghazi, 1994; El Sayed et al., 2004). They are unmetamorphosed and are mainly of intermediate to felsic composition with medium- to high-K calc-alkaline nature. Their tectonic setting is uncertain and may reflect subduction-related or extension- (rift-) related volcanism.

Field relations reveal that the Dokhan Volcanics postdate the calc-alkaline I-type Older Granites, but predate or are associated with the A-type Younger Granites (El Ramly, 1972; El Shazly, 1977; Akaad and Noweir, 1980). Stern and Gottfried (1986) argued that Dokhan rhyolites west of Safaga are extrusive equivalents of the Younger Granites. Some workers considered that the Dokhan Volcanics are older than the Hammamat molasse sediments (El Shazly, 1977), while others considered that the deposition of the Hammamat was synchronous with eruption of the Dokhan Volcanics (Ressetar and Monard, 1983; Ries et al., 1983). These observations are consistent with the overlap of whole rock Rb–Sr ages; 610–560 Ma for the Dokhan, 600–585 Ma for the Hammamat, and 610–550 Ma for the Younger Granites (Stern, 1979; Stern and Hedge, 1985; Bentor, 1985; Willis et al., 1988; Beyth et al., 1994; Jarrar et al., 2003). Recent SHRIMP zircon dating gave weighted U–Pb ages of 593 ± 13 and 602 ± 9 Ma for two andesites from the Dokhan Volcanics (Wilde and Yossef, 2000).

2.2. Local geology

The study area is located approximately 50 km northwest of Hurghada along the western coast of the Red Sea (Fig. 1a). It is underlain mainly by the Dokhan Volcanics and both Older and Younger Granites (Fig. 1b). In this area, the Dokhan Volcanic rocks cover about 110 km^2 including north of Gebel Dokhan along Wadi Um Sidra and further north along Wadi Um Asmer. The Older Granites are the oldest rocks and comprise quartz diorite, granodiorite, and adamellite. These granitic rocks have not been dated in the area but at Mons Claudianus to the south are ~670 Ma (Stern and Hedge, 1985). The Dokhan Volcanics overlie, intrude, and occasionally contain xenoliths of the Older Granites. All the volcanics are assigned to the typical Dokhan Volcanics, not to the OMV as previously reported at Gebel Kherm Asmer (Ghanem et al., 1973; Abu El Leil, 1980). The Younger Granites in this area comprise perthitic biotite–granite and intrude the Dokhan Volcanics with sharp contacts and chilled margins of up to 30 cm thick. This clearly shows that intrusion of the Younger Granites continued after emplacement of the Dokhan Volcanics in this area.

The Dokhan Volcanics are a stratified succession that varies in thickness from a few tens of meters up to more than 1000 m. Individual lava flows are about 10 m thick. The most conspicuous feature is the varicolored nature of lava flows ranging from gray to red and deep purple. Lavas are commonly porphyritic. The most abundant rocks are andesites, dacites, rhyodacites, and rhyolites. Basaltic rocks are scarce, and in many cases are only found at the base of the succession. Pyroclastic rocks occur as thin layers up to 1 m thick. They are intercalated

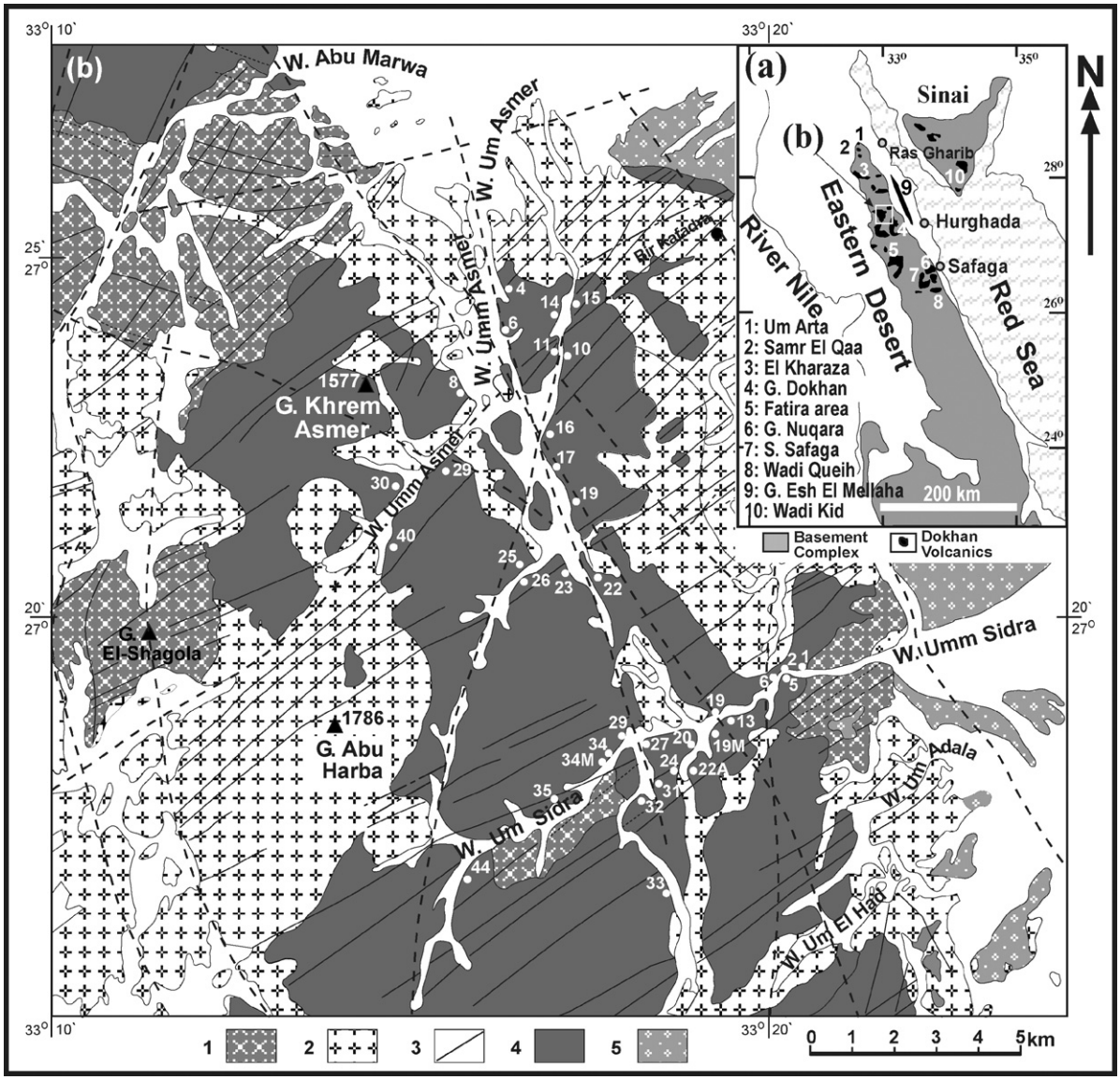

Fig. 1. (a) Distribution of the Dokhan Volcanics in the Eastern Desert and Sinai (after Abdel Rahman, 1996) and (b) geological map of the Wadi Um Sidra and Wadi Um Asmer area, NED, Egypt (modified after Abu El Leil, 1980). (1) Granodiorite-quartz diorite, (2) biotite hornblende granites and adamellite, (3) biotite granite, (4) perthitic granite, (5) granitic and granosyenite dykes, (6) diabasic dykes, (7) doleritic and dioritic dykes, (8) Dokhan Volcanics, (9) recent deposits. The numbers refer to the analyzed samples labeled AS and US along Wadi Um Asmer and Um Sidra, respectively.

between lava flows and commonly include fragments of the lavas. Although the Dokhan Volcanics are sometimes jointed and faulted, there is no evidence for folding.

3. Petrography

Basalts and basaltic andesites consist of plagioclase, amphibole, and augite phenocrysts in a fine-grained groundmass. Plagioclase is ubiquitous as tabular to prismatic (up to 0.5 cm) phenocrysts of labradorite to andesine ($An_{65–40}$). Augite phenocrysts are equant, simply twinned, and variably altered to actinolite. The common accessories are ilmenite, few magnetite and apatite.

Andesites are porphyritic, and occasionally show flow-banding and glomeroporphyritic textures. Plagioclase and amphibole are the main phenocrysts in a fine-grained groundmass. Euhedral to subhedral, tabular and prismatic phenocrysts of andesine ($An_{35–48}$) constitute about 25 modal percent of the lava. Hornblende phenocrysts constitute about 10 modal percent of the lava.

Ilmenite, magnetite, apatite, and zircon are the accessories, while epidote, sericite, and chlorite are the secondary minerals.

Dacites consist of oligoclase ($An_{32–20}$), hornblende, biotite, and quartz phenocrysts in a fine-grained groundmass. Hornblende forms euhedral prismatic phenocrysts. Graphic intergrowths are present. Magnetite, hematite, apatite, zircon, and titanite are common accessories. Kaolinite, sericite, chlorite, and epidote are secondary minerals.

Rhyodacites have phenocrysts of euhedral K-feldspar, tabular oligoclase ($An_{27–15}$) and subhedral quartz with biotite microphenocrysts in a devitrified groundmass. Magnetite, few ilmenite and apatite are the common accessories, while secondary minerals are sericite, muscovite, kaolinite, and epidote.

Rhyolites contain Carlsbad twinned K-feldspar and quartz phenocrysts with minor plagioclase microphenocrysts in a fine-gained groundmass. Spherulites are common. Accessories are hematite, apatite, fluorite, and zircon, while secondary minerals are kaolinite, chlorite, and sericite.

4. Geochemistry

4.1. Analytical methods

Thirty-five samples of the Dokhan Volcanics have been analyzed using the Rigaku RIX 2000 XRF instrument at the Department of Geoscience, Shimane University, Japan. The analyses were carried out according to the method of Kimura and Yamada (1996). Major and trace elements were analyzed using fused glass disks. To check analytical accuracy, a geostandard basalt sample JB-1 (Geological Survey of Japan) was analyzed every five samples. The analytical reproducibility was better than 2% for major and 5% for trace elements. Electron microprobe analysis (EPMA) on minerals was carried out using a JEOL JXA-8900 housed at Okayama University of Science, Japan and equipped with four wavelength-dispersive spectrometers and one energy-dispersive spectrometer. The operating conditions were a beam diameter of 3–5 μm, a beam current of 20 nA, and an accelerating voltage of 15 kV. Daily checks of analyses were made by analyzing natural and synthetic silicates and oxides, and the ZAF program was used for corrections.

Fourteen samples were chosen for rare earth element (REE) analysis using a combined alkali fusion and acid digestion procedure (Roser et al., 2000). The samples were analyzed following techniques described by Kimura et al. (1995) using an ICP-MS equipped with a normal concentric and a water chilled impact bead-type nebulizer. Analytical precision was better than ±4% for most elements. Instrument settings were fundamentally those reported by Kimura et al. (1995). All analyses were carried out at the Department of Geoscience, Shimane University, Japan. Major, trace, and rare earth elements are listed in Tables 1 and 2.

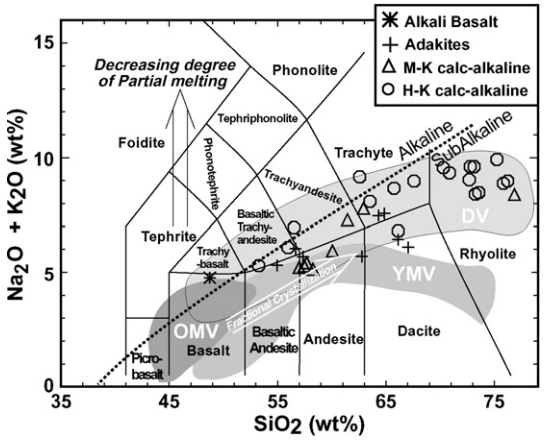

Fig. 2. Geochemical classification of Dokhan Volcanics on the total alkalis-silica (TAS) diagram (Le Maitre, 1989). For comparison, fields are also shown for Older and Younger metavolcanics (OMV and YMV) from Stern (1981), and Dokhan Volcanics (DV) from other areas (Basta et al., 1980; Ressetar and Monard, 1983; Stern and Gottfried, 1986; Abdel Rahman, 1996; Eliwa, 2000; Moghazi 1994, 2003).

4.2. Results

Geochemical classification using total alkali versus silica (TAS) diagram (Le Maitre, 1989) shows that the lavas studied are basalt, basaltic andesite, andesite, dacite, rhyodacite, and rhyolite (Fig. 2). The lavas plot mostly in the subalkaline field except for three samples which plot within the alkaline field of Irvine and Barager (1971) (Fig. 2). Sample US-24 is an alkali basalt, and trace element chemistry differs from other calc-alkaline suites (see Section 5). On the K_2O–SiO_2 diagram (Fig. 3) of Le Maitre (1989), the lavas are classified into medium-K (MK) and high-K (HK) suites with more high-K affinities in evolved dacite to rhyolite lavas.

As proposed by Defant and Drummond (1990, 1993), certain geochemical characteristics including Y (<18 ppm), Sr (>400 ppm), HREE (Yb < 1.9 ppm), Sr/Y (>40), and Al_2O_3 (>15 wt.%) can be used to discriminate between normal calc-alkaline lavas and adakites. On these bases, eight Dokhan lavas are adakite (Fig. 4a–c). The adakitic lavas belong to both the low-silica adakite (LSA) and high-silica adakite (HSA) groups of Martin and Moyen (2003). All adakitic lavas are relatively low

Table 1
Major elements composition and CIPW of the Dokhan Volcanics of Umm Sidar-Kherm Asmer area

	Sample no.																	
	US-24 B-*AK*[a]	US-44 BA-*CA*[a]	AS-30 BA-*AD*[a]	US-1 BA-*CA*[a]	AS-8 BA-*CA*[a]	US-19 BA-*AD*[a]	AS-16 A-*CA*[a]	US-19M A-*AD*[a]	AS-15 A-*CA*[a]	AS-10 A-*CA*[a]	AS-14 A-*CA*[a]	AS-40 A-*CA*[a]	US-20 A-*CA*[a]	AS-17 A-*CA*[a]	AS-4 A-*AD*[a]	US-32 A-*CA*[a]	AS-22 D-*CA*[a]	US-31 D-*AD*[a]
SiO_2	48.83	53.32	55.01	56.02	56.56	56.71	57.04	57.39	57.50	57.73	58.32	60.10	61.49	62.62	62.81	62.95	63.55	64.34
TiO_2	2.45	2.12	1.30	1.35	1.32	1.26	1.13	1.20	1.14	1.47	1.21	1.22	1.30	1.14	0.96	1.00	1.00	0.86
Al_2O_3	15.98	15.66	15.33	15.31	16.81	16.58	18.02	16.92	17.96	19.08	18.86	17.45	15.33	15.77	16.44	16.56	16.74	15.26
Fe_2O_3	12.76	10.58	8.91	8.41	8.06	8.27	8.48	7.92	8.29	9.85	9.57	8.45	6.72	5.22	7.27	5.79	5.46	5.08
MnO	0.18	0.21	0.12	0.12	0.10	0.13	0.09	0.11	0.09	0.10	0.09	0.11	0.08	0.11	0.05	0.10	0.12	0.07
MgO	6.58	5.24	7.05	5.05	3.40	2.58	2.68	2.42	2.65	1.76	1.85	2.12	3.20	2.04	1.14	1.87	0.84	2.79
CaO	7.77	7.01	6.36	6.56	5.90	7.24	6.49	7.21	6.37	4.12	4.43	4.25	3.93	3.17	5.10	3.51	3.62	3.60
Na_2O	2.70	3.11	3.72	3.72	4.67	3.64	4.19	3.33	4.16	3.79	3.80	3.89	5.05	4.71	4.50	5.33	4.89	4.67
K_2O	2.04	2.15	1.56	2.33	2.25	2.36	1.00	2.33	1.09	1.60	1.31	2.01	2.20	4.41	1.17	2.42	3.16	2.76
P_2O_5	0.48	0.38	0.31	0.43	0.45	0.39	0.30	0.37	0.29	0.29	0.31	0.24	0.37	0.36	0.34	0.34	0.33	0.25
L.O.I.	0.49	0.64	1.14	1.40	1.10	0.31	0.91	0.38	0.95	1.15	1.19	0.34	0.45	0.48	0.90	0.34	0.73	0.58
Total	100.26	100.42	100.81	100.70	100.62	99.47	100.33	99.58	100.49	100.94	100.94	100.18	100.12	100.03	100.68	100.21	100.44	100.26
$Mg^{\#}$	0.48	0.50	0.61	0.54	0.46	0.38	0.39	0.38	0.39	0.26	0.28	0.33	0.49	0.44	0.24	0.39	0.23	0.52
CIPW norm																		
Q	2.26	7.27	5.99	7.49	5.97	10.59	12.31	12.92	12.82	18.77	19.68	18.04	12.42	10.38	20.78	13.49	15.14	16.14
c	0.00	0.00	0.00	0.00	0.00	0.00	0.00	0.00	0.00	4.20	3.77	1.61	0.00	0.00	0.00	0.00	0.00	0.00
Or	12.10	12.73	9.23	13.80	13.31	13.96	5.92	13.78	6.45	9.47	7.76	11.90	13.02	26.11	6.93	14.33	18.70	16.34
Ab	22.84	26.31	31.47	31.47	39.51	30.80	35.45	28.17	35.20	32.07	32.15	32.91	42.73	39.95	38.07	45.10	41.37	39.51
An	25.49	22.47	20.58	18.24	18.32	22.00	27.47	24.41	27.18	18.92	20.31	19.88	12.70	8.90	21.29	14.16	14.46	12.58
Di	1.96	2.56	3.81	5.41	3.18	5.38	0.00	3.63	0.00	0.00	0.00	0.00	0.31	0.91	0.00	0.00	0.00	0.80
Hy	16.81	11.36	15.66	9.63	7.14	3.25	5.91	3.48	5.78	3.20	3.34	4.04	6.90	4.35	2.12	4.05	1.77	5.33
Hm	17.42	12.89	11.21	10.37	10.45	9.61	9.45	9.76	9.13	9.05	8.72	8.12	7.48	6.20	6.84	6.33	5.82	5.27
11	0.57	0.57	0.32	0.32	0.29	0.34	0.23	0.28	0.23	0.21	0.18	0.24	0.20	0.30	0.10	0.25	0.29	0.15
Tn	6.11	4.59	2.95	3.01	3.13	2.58	2.02	2.38	1.86	0.00	0.00	0.00	2.69	2.41	1.26	0.83	1.07	1.63

Table 1 (*Continued*)

	Sample no.																
	US-6 D-*AD*[a]	US-27 D-*CA*[a]	US-13 D-*AD*[a]	AS-23 D-*CA*[a]	US-34M D-*AD*[a]	US-2 D-*CA*[a]	AS-6 RD-*CA*[a]	US-5 RD-*CA*[a]	AS-11 RD-*CA*[a]	AS-29 RD-*CA*[a]	US-35 R-*CA*[a]	US-22A R-*CA*[a]	US-29 R-*CA*[a]	US-34 R-*CA*[a]	AS-25 R-*CA*[a]	AS-26 R-*CA*[a]	AS-19 R-*CA*[a]
SiO_2	64.90	65.77	66.13	66.15	67.08	67.60	72.69	72.77	70.30	70.88	75.83	73.14	73.58	73.26	75.24	76.24	76.85
TiO_2	0.83	0.99	0.78	0.92	0.85	0.70	0.38	0.43	0.60	0.42	0.11	0.42	0.37	0.37	0.10	0.14	0.19
Al_2O_3	14.36	15.61	15.14	16.13	14.08	15.40	14.46	14.35	15.20	14.42	12.63	14.14	13.89	14.08	12.78	12.51	12.39
Fe_2O_3	6.77	4.66	4.64	5.64	5.06	3.54	1.89	1.80	2.68	2.43	1.26	1.80	1.96	1.98	0.74	0.83	1.49
MnO	0.11	0.11	0.05	0.08	0.06	0.06	0.07	0.04	0.04	0.05	0.02	0.02	0.04	0.04	0.03	0.03	0.03
MgO	2.22	1.16	1.98	1.78	2.27	1.09	0.41	0.23	0.38	0.56	0.10	0.22	0.46	0.46	0.08	0.14	0.15
CaO	3.10	2.70	4.27	2.18	3.98	2.37	1.02	0.48	1.15	1.37	0.41	0.64	1.39	0.42	0.36	0.31	0.20
Na_2O	4.63	5.41	4.48	3.67	3.91	4.92	4.42	3.78	4.58	3.49	3.97	4.27	4.68	4.67	5.26	3.68	4.89
K_2O	2.89	3.21	1.92	3.10	2.16	4.01	4.57	5.79	4.94	5.80	4.86	5.29	3.75	3.69	4.62	5.26	3.45
P_2O_5	0.27	0.26	0.24	0.21	0.27	0.17	0.06	0.04	0.09	0.10	0.00	0.04	0.05	0.05	0.01	0.01	0.01
L.O.I.	0.88	0.24	0.31	0.81	0.53	0.18	0.10	0.54	0.12	1.01	1.18	0.36	0.32	0.83	0.55	0.59	0.32
Total	100.96	100.12	99.94	100.67	100.25	100.04	100.07	100.25	100.08	100.53	100.37	100.34	100.49	99.85	99.77	99.74	99.97
$Mg^{\#}$	0.39	0.33	0.46	0.39	0.47	0.38	0.30	0.20	0.22	0.31	0.14	0.20	0.32	0.32	0.18	0.25	0.17
CIPW norm																	
Q	18.43	15.75	22.09	26.03	25.57	17.84	26.71	27.20	21.79	24.70	33.03	26.32	28.57	30.40	28.18	33.78	34.53
c	0.00	0.00	0.00	3.15	0.00	0.00	0.44	0.99	0.32	0.03	0.07	0.23	0.00	1.68	0.00	0.18	0.26
Or	17.10	19.00	11.37	18.36	12.79	23.74	27.06	34.27	29.23	34.35	28.82	31.31	22.19	21.84	27.42	31.16	20.42
Ab	39.17	45.77	37.90	31.05	33.08	41.63	37.40	31.98	38.75	29.53	33.59	36.13	39.60	39.51	39.93	31.14	41.37
An	9.91	8.88	15.58	9.85	14.55	8.14	4.96	2.43	5.52	6.54	2.06	3.20	5.86	2.02	0.00	1.58	0.97
Di	0.91	0.10	1.00	0.00	0.57	0.42	0.00	0.00	0.00	0.00	0.00	0.00	0.00	0.00	0.27	0.00	0.00
Hy	3.86	2.37	3.13	2.93	3.61	1.98	0.70	0.39	0.71	0.99	0.15	0.38	0.76	0.73	0.00	0.21	0.23
Hm	6.65	4.91	4.29	4.69	4.38	3.59	1.62	1.53	2.51	2.18	0.99	1.56	1.64	1.59	0.00	0.64	1.13
11	0.23	0.27	0.10	0.15	0.11	0.13	0.13	0.07	0.08	0.10	0.04	0.03	0.07	0.07	0.06	0.05	0.05
Tn	1.40	1.82	1.34	0.00	1.94	1.29	0.00	0.00	0.00	0.00	0.00	0.00	0.46	0.00	0.11	0.00	0.00

[a] Rock type, B: basalt; BA: basaltic andesites; A: andesites; D: dacites; RD: rhyodacite; R: rhyolite; Ak: alkali; CA: normal calc-alkaline; AD: adakite.

Table 2
Trace and rare earth elements composition of the Dokhan Volcanics of Umm Sidar-Kherm Asmer area

	Sample no.																	
	US-24 B-*AK*[a]	US-44 BA-*CA*[a]	AS-30 BA-*AD*[a]	US-1 BA-*CA*[a]	AS-8 BA-*CA*[a]	US-19 BA-*AD*[a]	AS-16 A-*CA*[a]	US-19M A-*AD*[a]	AS-15 A-*CA*[a]	AS-10 A-*CA*[a]	AS-14 A-*CA*[a]	AS-40 A-*CA*[a]	US-20 A-*CA*[a]	AS-17 A-*CA*[a]	AS-4 A-*AD*[a]	US-32 A-*CA*[a]	AS-22 D-*CA*[a]	US-31 D-*AD*[a]
Ba	487	687	436	612	715	754	495	693	551	600	513	544	447	920	702	606	802	644
Cr	35	171	366	198	134	109	18	93	21	38	28	47	19	35	96	6	32	126
Ni	70	67	157	74	63	67	20	60	19	15	15	32	15	26	45	6	14	31
Pb	6	8	6	6	10	13	14	9	14	9	6	5	18	10	9	7	11	9
V	308	256	179	186	189	175	188	172	183	216	189	174	118	91	148	101	58	52
Rb	112	71	21	63	42	27	18	26	22	45	46	52	47	105	26	58	66	58
Sr	724	687	849	703	847	1073	728	991	733	591	602	587	573	498	1019	372	524	774
Ga	22	17	19	19	21	19	21	19	21	23	21	23	20	19	18	19	19	19
Nb	18	14	9	12	11	6	11	8	11	13	11	15	14	37	6	12	13	10
Th	2	2	3	9	4	4	4	2	4	4	3	2	5	11	3	6	5	3
Y	32	24	17	20	28	15	28	15	27	31	28	28	23	27	14	26	33	16
Zr	233	187	173	190	203	165	194	153	195	230	180	178	284	391	141	243	254	182
Li[b]	12.28	24.03		26.47	13.95	2.78	16.79			22.80				9.17	8.18	25.52		
Be[b]	1.66	1.59		1.70	1.43	1.20	1.23			1.26				2.26	1.08	1.48		
Sb[b]	0.54	1.00		1.13	5.40	4.96	0.50			1.26				0.44	6.78	0.37		
Hf[b]	4.24	2.25		5.43	4.33	3.90	4.51			4.85				6.97	2.70	5.24		
Ta[b]	0.69	1.51		1.13	0.46	0.39	0.84			0.91				4.38	0.36	1.05		
U[b]	1.83	0.49		0.56	1.12	0.91	1.11			1.10				3.14	0.61	1.91		
La	25.08	21.21		22.55	24.97	23.56	20.18			22.32				39.25	15.84	26.00		
Ce	55.57	53.64		56.70	55.95	51.92	45.45			49.92				75.92	38.59	56.82		
Pr	6.80	7.01		7.58	7.32	6.68	5.79			6.43				9.21	4.92	7.01		
Nd	27.37	32.19		33.20	31.59	28.20	24.74			28.12				34.06	20.44	28.08		
Sm	5.11	6.84		7.42	6.34	5.54	5.13			5.73				6.04	3.99	5.55		
Eu	1.53	2.11		2 27	1.94	1.74	1.52			1.70				1.73	1.29	1.39		
Gd	4.03	6.37		6.98	5.20	4.44	4.72			5.14				4.82	3.03	4.75		
Tb	0.55	0.90		1.01	0.73	0.58	0.69			0.73				0.67	0.40	0.65		
Dy	2.97	5.20		5.51	4.22	3.16	4.19			4.19				3.86	2.24	3.89		
Ho	0.52	0.94		1.03	0.77	0.55	0.83			0.81				0.69	0.41	0.70		
Er	1.24	2.32		2.59	2.07	1.33	2.17			2.04				1.79	1.03	1.84		
Tm	0.18	0.34		0.37	0.32	0.18	0.33			0.31				0.27	0.16	0.29		
Yb	1.03	2.07		2.07	1.95	0.99	2.18			2.03				1.79	1.00	1.85		
Lu	0.18	0.29		0.34	0.34	0.17	0.33			0.31				0.26	0.15	0.28		
La_N/Lu_N	14.27	7.43		6.80	7.49	14.42	6.30			7.50				15.27	11.06	9.43		
La_N/Sm_N	3.03	1.91		1.87	2.43	2.62	2.43			2.40				4.01	2.45	2.89		
Gd_N/Lu_N	2.73	2.66		2.51	1.86	3.24	1.76			2.06				2.23	2.52	2.05		
Zr/Nb	0.08	0.07	0.05	0.06	0.05	0.04	0.06	0.05	0.06	0.06	0.06	0.08	0.05	0.09	0.04	0.05	0.05	0.05
Rb/Zr	0.48	0.38	0.12	0.33	0.21	0.16	0.09	0.17	0.11	0.20	0.26	0.29	0.17	0.27	0.18	0.24	0.26	0.32
Sr/Y	23	29	50	35	30	72	26	66	27	19	22	21	25	18	73	14	16	48
Ti/Zr	63	68	45	43	39	46	35	47	35	38	40	41	27	17	41	25	24	28

Table 2 (*Continued*)

	Sample no.																
	US-6 D-*AD*[a]	US-27 D-*CA*[a]	US-13 D-*AD*[a]	AS-23 D-*CA*[a]	US-34M D-*AD*[a]	US-2 D-*CA*[a]	AS-6 RD-*CA*[a]	US-5 RD-*CA*[a]	AS-11 RD-*CA*[a]	AS-29 RD-*CA*[a]	US-35 R-*CA*[a]	US-22A R-*CA*[a]	US-29 R-*CA*[a]	US-34 R-*CA*[a]	AS-25 R-*CA*[a]	AS-26 R-*CA*[a]	AS-19 R-*CA*[a]
Ba	656	863	414	841	602	888	837	951	1010	983	37	857	716	723	63	309	96
Cr	133	4	79	76	115	42	22	29	19	19	53	40	41	42	55	38	37
Ni	31	20	18	47	45	15	3	5	5	16	39	3	7	7	26	6	2
Pb	9	13	7	13	9	13	15	17	14	14	25	12	35	34	19	17	5
V	92	49	81	108	105	71	13	22	47	35	n.d.	32	17	22	n.d	6	11
Rb	54	62	47	94	59	106	119	135	96	175	260	125	77	77	301	189	76
Sr	677	396	767	509	816	557	183	158	362	352	48	154	192	194	7	55	43
Ga	17	21	20	21	18	19	17	20	19	19	20	20	14	12	29	17	20
Nb	9	16	10	14	10	13	17	18	13	22	55	17	12	13	42	17	18
Th	6	6	5	7	4	7	10	10	7	16	29	4	11	13	41	22	13
Y	15	36	16	22	15	19	31	23	20	33	58	23	18	18	21	15	32
Zr	167	346	171	247	166	305	346	441	357	280	197	446	296	298	135	99	309
Li[b]	13.09							7.63	8.70						4.26		
Be[b]	2.50							2.29	2.01						4.62		
Sb[b]	0.47							0.49	1.40						0.40		
Hf[b]	3.95							10.72	8.49						5.30		
Ta[b]	0.67							1.29	0.91						2.62		
U[b]	1.68							3.69	2.50						12.94		
La	21.38							40.35	36.05						31.82		
Ce	48.29							84.21	77.69						50.98		
Pr	5.93							9.91	9.36						4.28		
Nd	24.52							38.12	37.08						10.09		
Sm	4.67							6.30	6.28						1.36		
Eu	1.41							1.15	1.48						0.03		
Gd	3.57							4.81	4.63						1.11		
Tb	0.50							0.69	0.65						0.22		
Dy	2.72							4.07	3.49						1.60		
Ho	0.49							0.72	0.62						0.40		
Er	1.22							1.98	1.54						1.44		
Tm	0.18							0.32	0.24						0.31		
Yb	0.98							1.79	1.31						2.26		
Lu	0.17							0.30	0.24						0.43		
La_N/Lu_N	12.69							13.92	15.56						7.61		
La_N/Sm_N	2.82							3.95	3.54						14.45		
Gd_N/Lu_N	2.53							1.98	2.38						0.32		
Zr/Nb	0.05	0.05	0.06	0.06	0.06	0.04	0.05	0.04	0.04	0.08	0.28	0.04	0.04	0.04	0.31	0.17	0.06
Rb/Zr	0.32	0.18	0.27	0.38	0.36	0.35	0.34	0.31	0.27	0.63	1.32	0.28	0.26	0.26	2.23	1.91	0.25
Sr/Y	45	11	48	23	54	29	6	7	18	11	1	7	11	11	0	4	1
Ti/Zr	30	17	27	22	31	14	7	6	10	9	3	6	7	7	4	8	4

[a] Rock type.
[b] Analysis by ICP, n.d.: not detected.

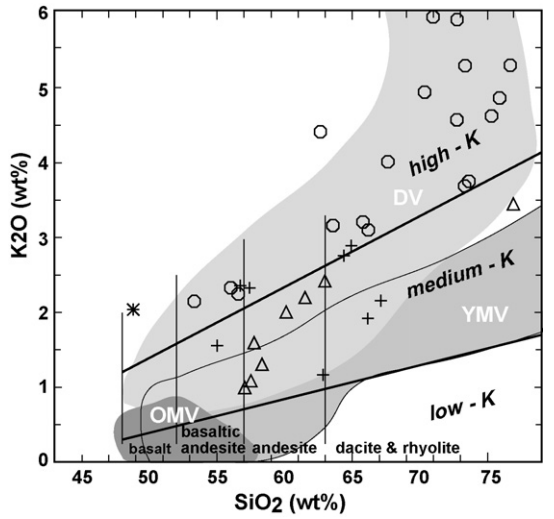

Fig. 3. SiO_2 vs. K_2O diagram (Le Maitre, 1989). HK: high-K; MK: medium-K; CA: calc-alkaline; Alk Bas: alkali basalt; HK CA: high-K calc-alkaline volcanics; MK CA: medium-K calc-alkaline. Fields for OMV, YMV, and Dokhan as in Fig. 2.

in K_2O, ranging from low- to medium-K boundary to slightly higher than medium- to high-K boundary lines (Fig. 3). Overall, the study lavas from the Dokhan Volcanics can be classified into minor (1) alkali basalt, (2) voluminous calc-alkaline medium-K to high-K andesite to rhyolite, and (3) subordinate adakite suites.

The calc-alkaline Dokhan Volcanics lavas vary from basaltic andesite (53% SiO_2) to rhyolite (76.9% SiO_2). All major elements but K_2O and Na_2O decrease with increasing SiO_2 content (Fig. 5). Al_2O_3 demonstrates little (non-systematic) variations over 48–63% SiO_2 range. TiO_2 content is distinctively high in the alkali basalt (2.45 wt.%). TiO_2 decreases in subalkaline (calc-alkaline) suite from andesite (1.47–0.96 wt.%; except sample US-44) through dacites (1.14–0.70 wt.%) to rhyodacites and rhyolites (0.60–0.10 wt.%). All Dokhan Volcanics have normative quartz and hypersthene; a few calc-alkaline lava that are Al_2O_3-rich have normative corundum (Table 1). Adakitic lavas are relatively low in Al_2O_3 and Na_2O, but have elevated MgO and CaO.

Cr and Ni decrease in calc-alkaline lavas, whereas Rb, Nb, Y, and Zr slightly increase or remain constant with increasing SiO_2 (Fig. 6). Rhyolite exhibits a wide range of high field strength elements (HFSE) contents (Y, Nb, and Zr), and large ion lithophile elements (LILE, e.g., Rb). Ba and Zr define a slight positive correlation trend over 48–73% SiO_2 range, but drop in rhyolites. Sr decreases with increasing silica over the entire compositional range. Cr, Ni, and Sr are relatively low in alkali basalt, whereas Nb, Rb, and Zr are high. Adakitic

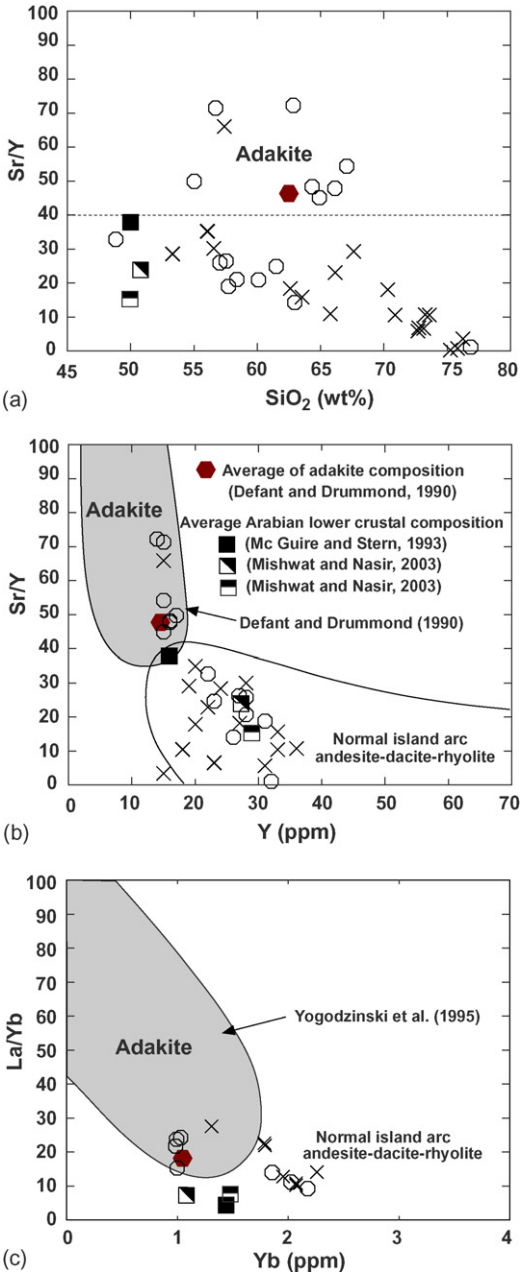

Fig. 4. Binary relations of adakites: (a) SiO_2 vs. Sr/Y, (b) Y vs. Sr/Y, and (c) Yb vs. La/Yb. Symbols as in Fig. 2.

lavas are commonly high in Cr, Ni, and Sr, whereas low in Y and Zr compared to calc-alkaline equivalents (Fig. 6).

Mid oceanic ridge basalt (MORB) normalized trace elements patterns are similar between alkali basalt, calc-alkaline basaltic andesite to andesite, and adakite, revealing a common enrichment of LILE, such as Rb, Ba, K, Pb, and Sr and the HFSE (Zr, Hf, and LREE). These pat-

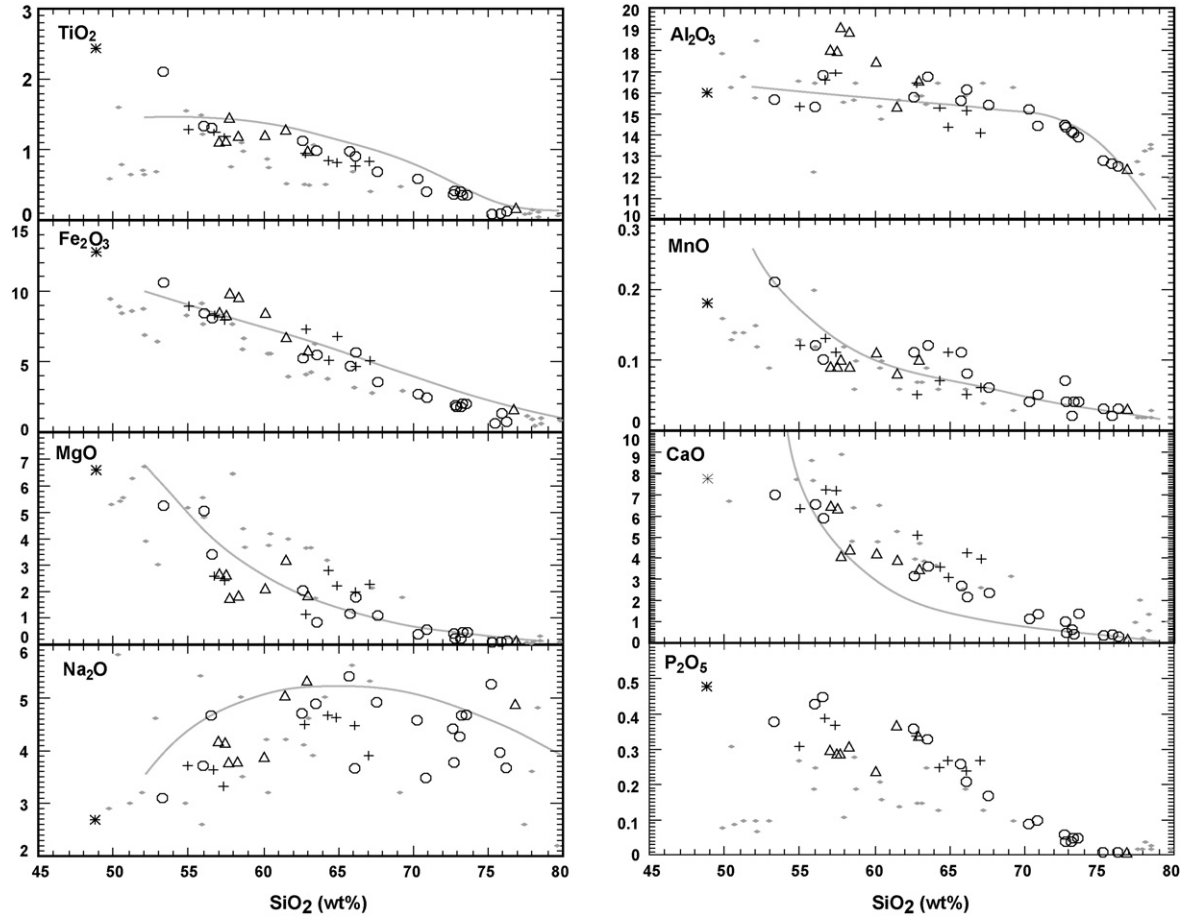

Fig. 5. Variations of major oxides against SiO_2 (wt.%) for the studied volcanics. The solid line is the average composition of the Dokhan Volcanics along Safaga-Qena road (Ressetar and Monard, 1983). For comparison, compositions of the Younger Metavolcanics (YMV; Stern, 1981) are plotted as dark grey dots (.). Symbols as in Fig. 2.

terns show negative Nb–Ta anomalies relative to LILE and LREE (Fig. 7). However, there are considerable differences between the suites.

Alkali basalt shows very small Nb–Ta negative anomaly with lower Th and nill Sr positive anomaly and fractionated REE region (Fig. 8), which are typical of alkali basalts in an arc environment.

Calc-alkaline suites have relatively flatter REE patterns with strong positive K, Pb, and Th anomalies. Interestingly, incompatible element abundances including REE in high-K basaltic andesite have almost identical element abundances with those in medium-K andesite. High-K dacite lavas have slightly fractionated REE patterns with more elevated light (L)REE and depleted heavy (H)REE than those in high-K basaltic andesite. Negative Eu anomaly in the felsic lavas suggests fractionation of hornblende with plagioclase from basaltic andesite of the same suite. Medium-K andesite suite basically has same trace element pattern with high-K basaltic andesite suite, suggesting the derivation of the magma from a similar source.

In contrast to the calc-alkaline suite lavas, adakitic lavas have steeper REE pattern and more Cr and Ni. Overall trace element abundances of Dokhan adakitic lavas are almost identical with the global average of adakitic lavas (Fig. 7).

A high-K calc-alkaline rhyolite (AS-25) shows strong depletion in Sr, Eu, Ti, and P, which probably reflects the fractionation of plagioclase, Fe–Ti oxides and apatite, respectively. Ba depletion in high-K calc-alkaline rhyolites is probably due to the fractionation of K-feldspar. The compositions of two rhyolites (AS-17 and AS-25) can be classified as A-type granitoids (e.g., Eby, 1992), indicating a relationship between Dokhan felsics and the Egyptian Younger Granites. They plot in the within-plate granite field of Pearce et al. (1984). They have an extremely high Nb–Ta anomalies (see Fig. 7), which make them distinct from other Dokhan calc-alkaline

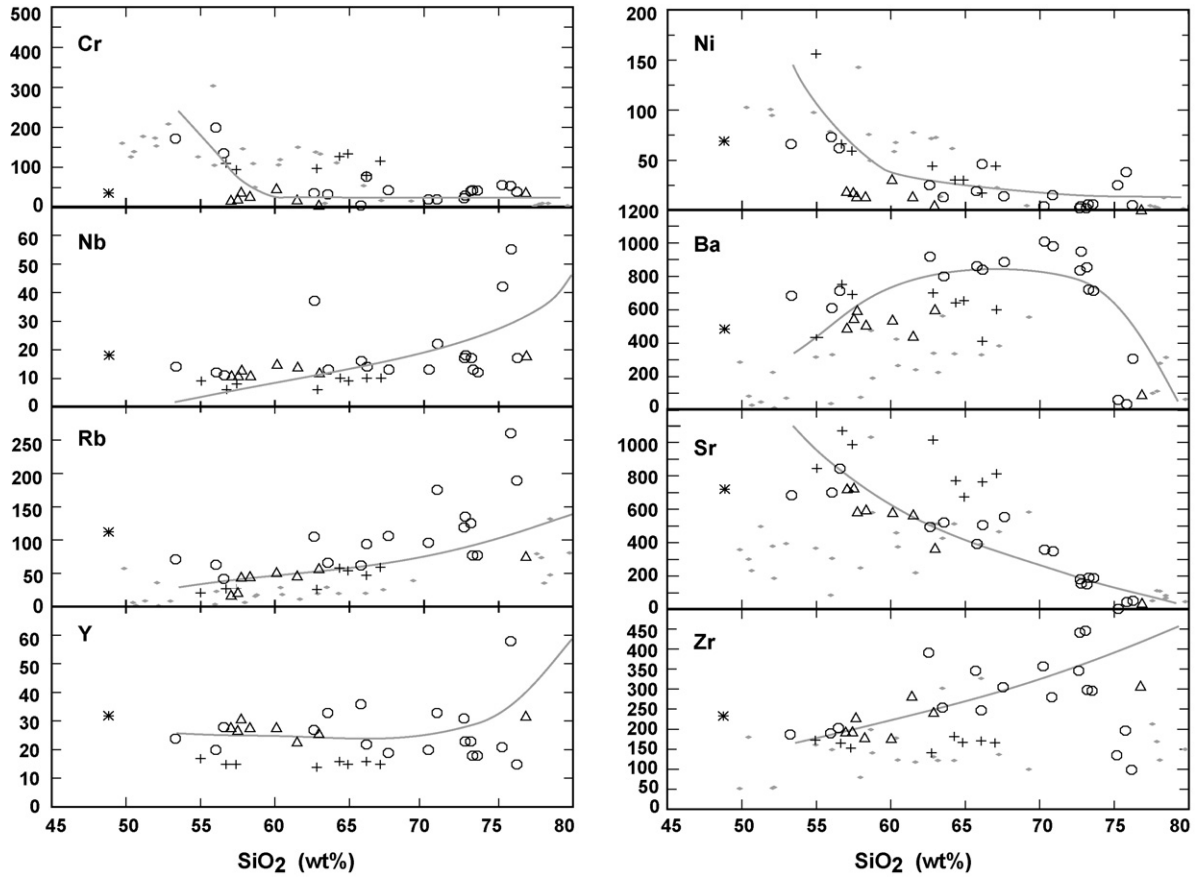

Fig. 6. Variation diagrams of some trace elements (ppm) against SiO_2 (wt.%) for the Dokhan Volcanics. The solid line is the average composition of the Dokhan Volcanics along the Safaga-Qena road (Ressetar and Monard, 1983). For comparison, compositions of the YMV (Stern, 1981) are plotted herein. Symbols are as in Fig. 2.

felsic lavas. REE patterns of these two rhyolite lavas are distinct: U-shaped with strong negative Eu anomaly for AS-25 and steep REE pattern with a weak negative Eu anomaly for AS-17. However, elevated HFSE together with depleted HREE (Nb/Y > 1.5) defines them as A_1-subtype of A-type granitoid. These characteristics are different from those in the Younger Granites (Moghazi et al., 1999; Mohamed et al., 1994) for which lower Nb–Ta and higher HREE classifying them as A_2-subtype. Therefore, origins of these two magma types differ (Eby, 1992).

5. Discussion

5.1. Is Dokhan volcanism bimodal?

There are different opinions about whether the Dokhan Volcanics represent a bimodal suite with silica gap between mafic and felsic rocks (Ressetar and Monard, 1983; Stern and Gottfried, 1986; Stern et al., 1988) or form a compositionally continuous suite (Basta et al., 1980; Abdel Rahman, 1996; Eliwa, 2000; Moghazi, 2003; El Sayed et al., 2004). Silica histograms of the Dokhan Volcanics from seven different localities in the Eastern Desert and Sinai are shown in Fig. 9. Silica contents from Dokhan Volcanics in different areas are compiled together with the volcanics studied (Fig. 9g). Much of the Dokhan Volcanics show no SiO_2 compositional gap, but a bimodal distribution is shown by samples from the Safaga-Qena and S. Safaga areas. These show two peaks at 55–60 and 70–80 wt.% SiO_2. It is not clear why the southernmost Dokhan localities are a bimodal suite whereas to the north the suite is not bimodal.

5.2. Tectonic setting of the Dokhan Volcanics

The study Dokhan Volcanics are plotted on tectonic discrimination diagrams (Fig. 10), which are based on virtually immobile elements (e.g., Zr, Ti, Y, and Nb).

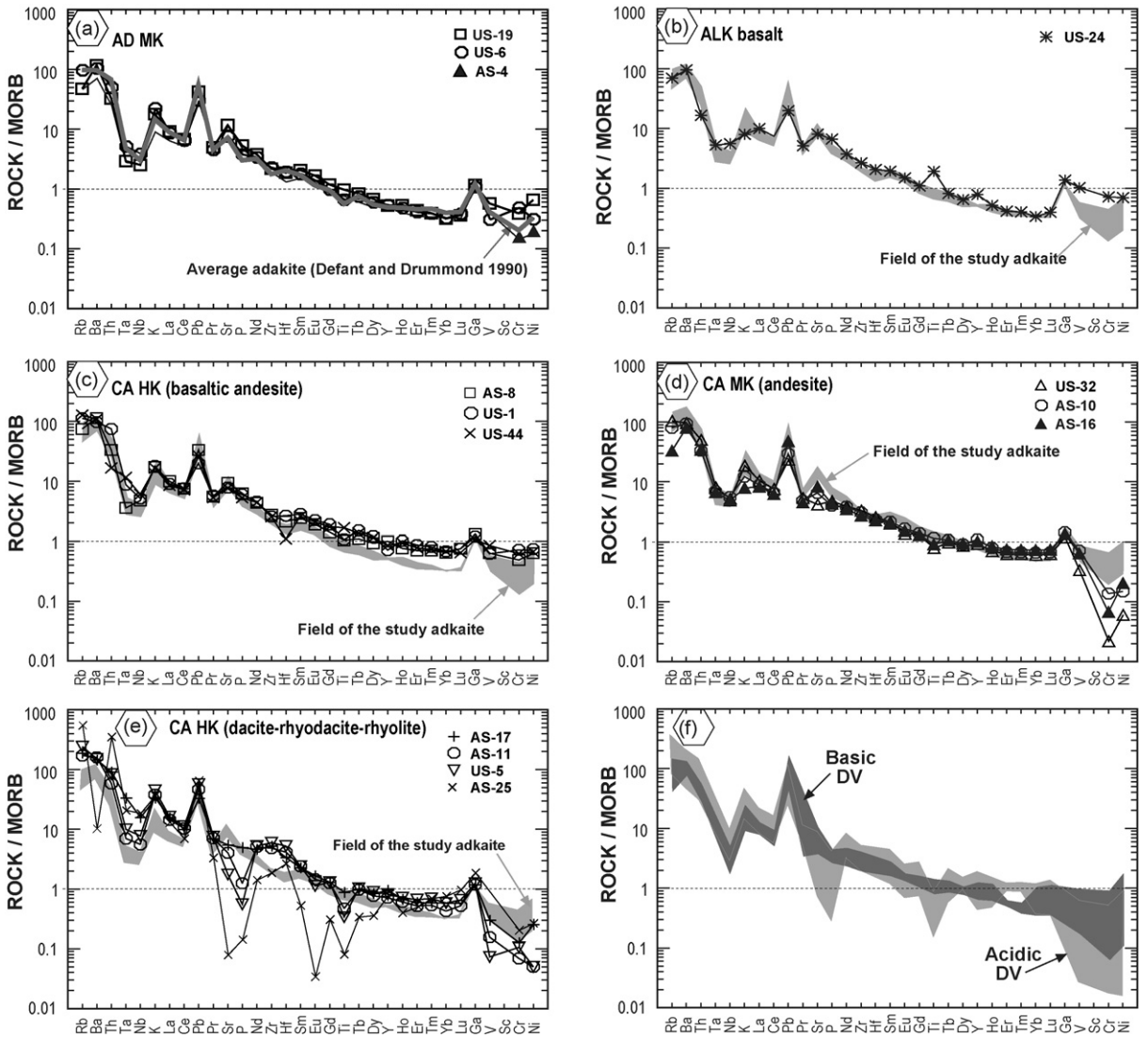

Fig. 7. N-MORB normalized diagrams of the Dokhan Volcanics: (a) medium-K Adakite, (b) alkali basalt, (c) calc-alkaline high-K basaltic andesites, (d) calc-alkaline medium-K andesite, (e) calc-alkaline high-K dacite–rhyodacite–rhyolite, and (f) fields of the basic and acidic Dokhan Volcanics (DV). Data sources for the Dokhan Volcanics are as in Fig. 2.

The OMV, YMV, and the Dokhan Volcanics from other areas are also shown for comparison. The mafic lavas plot on Ti/100–Zr–Sr/2 diagram in the field of "calc-alkaline basalts" typical of convergent plate margins (Fig. 10a). The felsic lavas plot in the "volcanic arc granite" field on the binary Y + Nb–Rb diagram of Pearce et al. (1984) (Fig. 10b), except for the rhyolite sample, which falls in the deeper "within-plate" field (Fig. 10b). A ternary K_2O–TiO_2–P_2O_5 diagram illustrates that the investigated Dokhan Volcanics erupted in a continental rather than in oceanic setting (Fig. 10d). The Dokhan lavas mostly plot in an overlap zone between the volcanic arc and within plate settings on the binary SiO_2–Nb diagram of Pearce and Gale (1977) (Fig. 10d), suggesting a transitional tectonic setting. These diagrams mostly indicate that the Dokhan Volcanics erupted in an arc environment with thicker (continental) crust.

In the Neoproterozoic evolution of the Egyptian basement complex, the obduction of ophiolite complexes and accretion of island arc terrane took place during the first tectono-magmatic episode (ca. 720–700 Ma) (Harms et al., 1994; Kröner et al., 1994; Stern, 1994, 2002), while the accreted terrane collided with the west Saharan Craton during the second episode (ca. 650–620 Ma) (Schandelmeier et al., 1987; Kröner et al., 1994; Sultan et

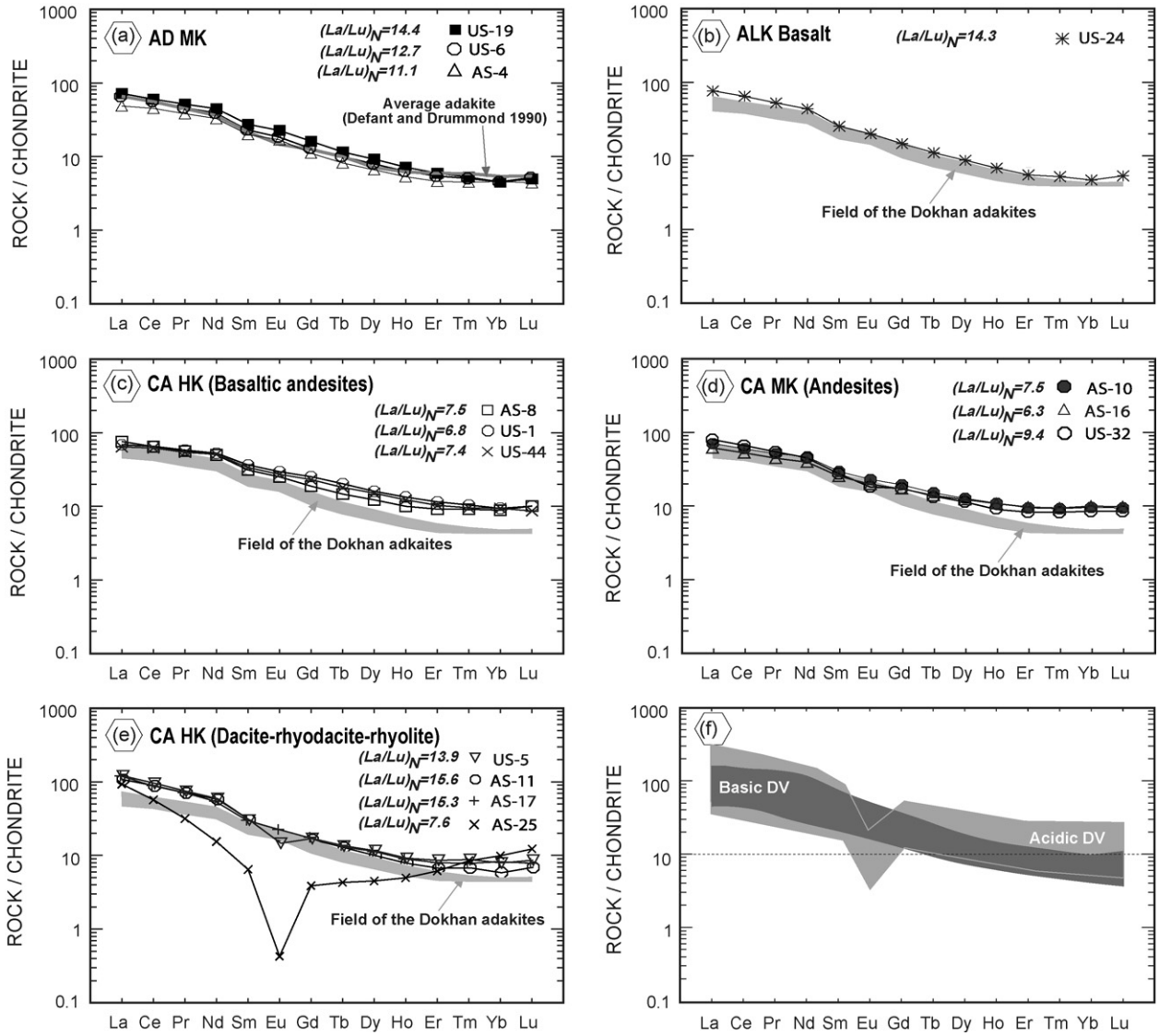

Fig. 8. Rare earth element patterns of the studied volcanics: (a) medium-K adakite, (b) alkali basalt, (c) high-K calc-alkaline basaltic andesites, (d) medium-K calc-alkaline, (e) high-K calc-alkaline dacite-rhyodacite-rhyolite, and (f) fields of the basic and acidic Dokhan Volcanics (DV). Data sources for the Dokhan Volcanics are as in Fig. 2.

al., 1994). Greiling et al. (1994) suggested that collision ended at ca. 615–600 Ma and the extensional collapse started sometime between 600 and 575 Ma. The eruption of the 600–590 Ma Dokhan Volcanics took place at the transition between collision and extension. The Dokhan Volcanics often lack bimodality, and possess arc geochemical signatures as noted above. The arc-related geochemical characteristics suggest that subduction continued until near end of the collision stage beneath the Dokhan Volcanics province, or that the mantle source retained a geochemical memory of subduction-related modifications. A-type like rhyolite lavas occur in the Dokhan Volcanics and have slightly different geochemical characteristics than post-Dokhan Younger Granites. In summary, the Dokhan Volcanics erupted during the transition from subduction-related magmatism to extension-related magmatism; slightly after the terminal collision between E and W Gondwana occurred and starting the extension.

5.3. Petrogenesis

The close association of the Dokhan "common" calc-alkaline and adakitic lavas has not been recognized pre-

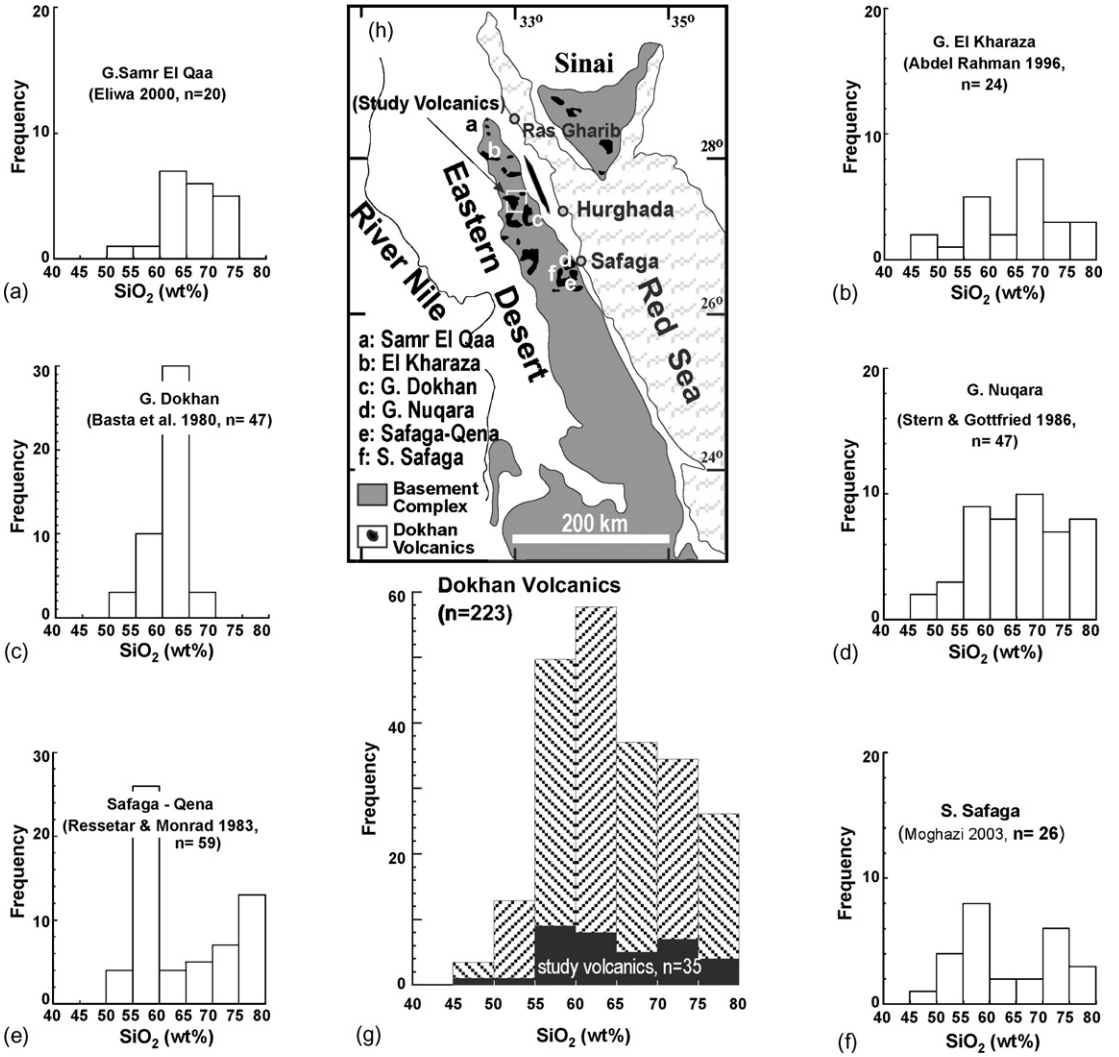

Fig. 9. Histograms showing SiO_2 (wt.%) distribution for the Dokhan Volcanics from different areas in Egypt: (a) G. Samr El Qaa (Eliwa, 2000); (b) G. El Kharaza (Abdel Rahman, 1996); (c) G. Dokhan (Basta et al., 1980); (d) G. Nuqara (Stern and Gottfried, 1986); (e) Safaga-Qena road (Ressetar and Monard, 1983); (f) S. Safaga area (Moghazi, 2003); (g) the studied volcanics compared to data of the Dokhan Volcanics compiled herein, and (h) distribution map of the Dokhan Volcanics provinces used for comparison.

viously in the Arabian–Nubian Shield, although adakitic rocks have been recognized in central Arabia (Hargrove et al., 2004). Sr/Y is a good discrimination parameter for intermediate lavas and there are sufficient published data so that it is useful to see if there are adakites in the Dokhan Volcanics in the other areas. Plots of Sr/Y against latitude for intermediate Dokhan lavas show that adakitic lavas are common in the study area and to the south but not north of 27°50′N (Fig. 11). "Common" calc-alkaline lavas dominate, regardless of whether adakites are present or absent. However, Fig. 11 shows that adakitic calc-alkaline lavas are the common characteristics of the Dokhan Volcanics, and the area shares the core part of the volcanic provinces over an area of 150 km × 50 km extending NNW-SSE. Alkali basalts (high Ti) are found in some areas (e.g., G. Nuqara, Stern and Gottfried, 1986; G. Kharaza; Abdel Rahman, 1996) to the south as well.

5.3.1. *Origin of the adakitic lavas*

Adakites are intermediate to felsic rocks whose compositions range from mafic andesite to dacite and rhyolite; basaltic members are lacking (Defant and Drummond, 1990; Maury et al., 1996; Martin, 1999). In these lavas, phenocrysts are mainly zoned plagioclase, hornblende, and biotite; orthopyroxene and clinopyroxene phenocrysts are found in mafic andesites (Kay, 1978; Rogers et al., 1985; Calmus et al., 2003).

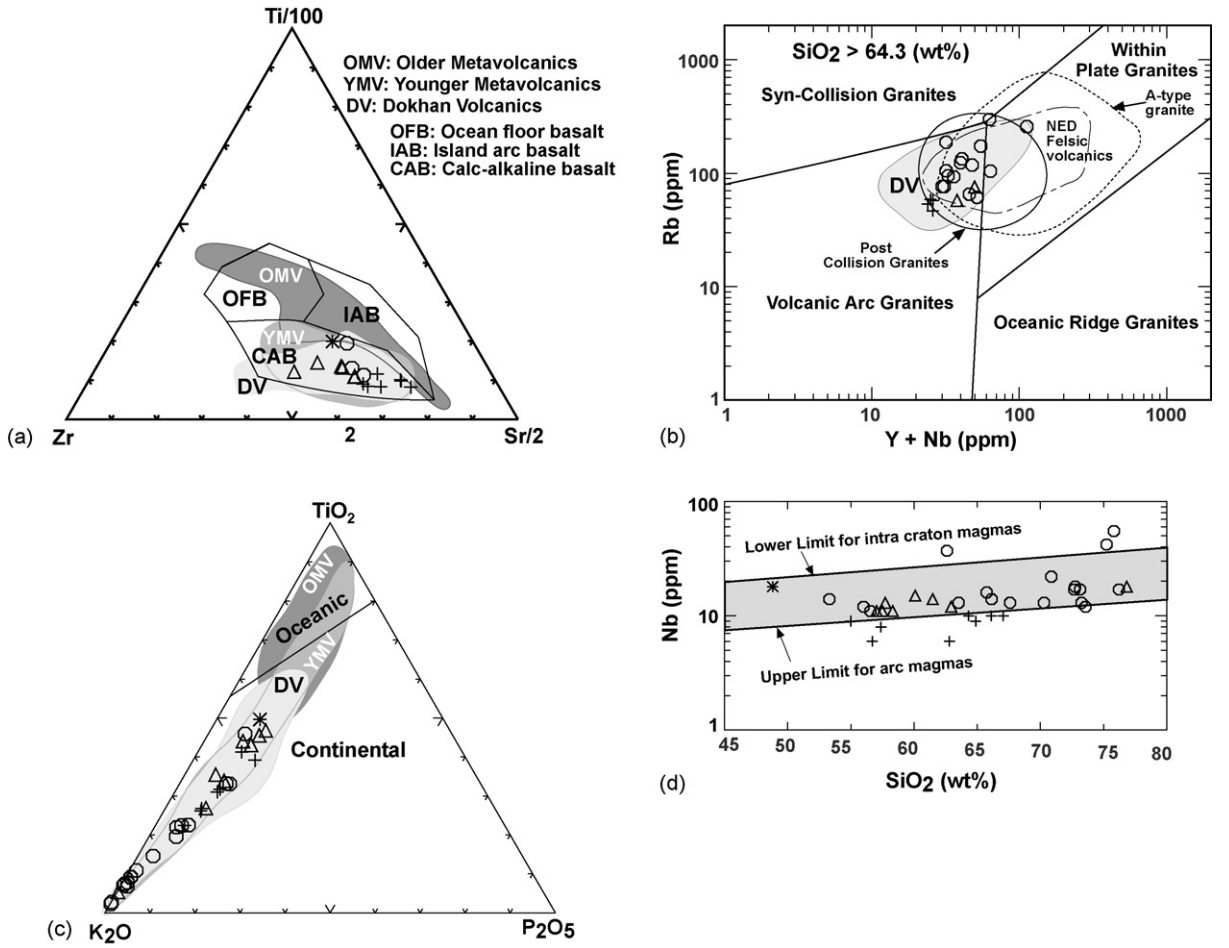

Fig. 10. Discrimination diagrams illustrating tectonic setting of the studied volcanics: (a) Zr–Ti/100–Sr/2 (Pearce and Cann, 1973), (b) Yb + Nb vs. Rb (Pearce et al., 1984), (c) K_2O–TiO_2–P_2O_5 (Pearce et al., 1975), and (d) SiO_2 vs. Nb diagram (Pearce and Gale, 1977). Post-COLG: post-collision granites (Pearce et al., 1984), NED volcanics (Stern and Gottfried, 1986), A-type granites (Whalen et al., 1987). Fields for comparison and symbols are as in Fig. 2.

Accessory phases are apatite, zircon, sphene, and titanomagnetite. Adakites have $SiO_2 > 56$ wt.%, high Na_2O contents (3.5 wt.% $\leq Na_2O \leq$ 7.5 wt.%), and low K_2O/Na_2O (~0.42). Their $Fe_2O_3 + MgO + MnO + TiO_2$ contents are moderately high (~7 wt.%), with high $Mg^{\#}$ (~0.51) and moderately high Ni and Cr contents (24 and 36 ppm, respectively). Defant and Drummond (1990) also reported typically high Sr contents (>400 ppm), with extreme concentrations reaching 3000 ppm. REE patterns are strongly fractionated ($(La/Yb)_N > 10$) with typically low HREE contents (Yb < 1.8 ppm, Y < 18 ppm). Amongst the defining geochemical characteristics of adakites are their steep REE patterns, low Y, and high Sr contents; two widely used discriminant diagrams are $(La/Yb)_N$ versus Yb_N (Martin, 1987, 1999) (where subscript N indicates chondrite normalization), and Sr/Y versus Y (Defant and Drummond, 1990). Using these indicators, some of the lavas in the Dokhan Volcanics are typical adakite as shown in Fig. 4.

Martin and Moyen (2003) and Martin et al. (2005) identified two distinct adakite groups: high-SiO_2 adakites (HSA; $SiO_2 > 60$ wt.%) and low-SiO_2 adakites (LSA; $SiO_2 < 60$ wt.%). From the study area, two adakites are LSA and six are HSA. However, trace element characteristics of the two Dokhan suites do not correlate well with the discrimination proposed by Martin et al. (2005). We therefore deal with the Dokhan LSA and HSA together to examine their petrogenesis.

Many studies infer the generation of adakitic magmas by melting of subducted eclogitic oceanic crust at high pressure (Kay, 1978; Defant and Drummond, 1990; Yogodzinski et al., 2001). Others (Hildreth and Moorbath, 1988; Feeley and Hacker, 1995; Smithies, 2000; Whalen et al., 2002) have suggested that adakitic

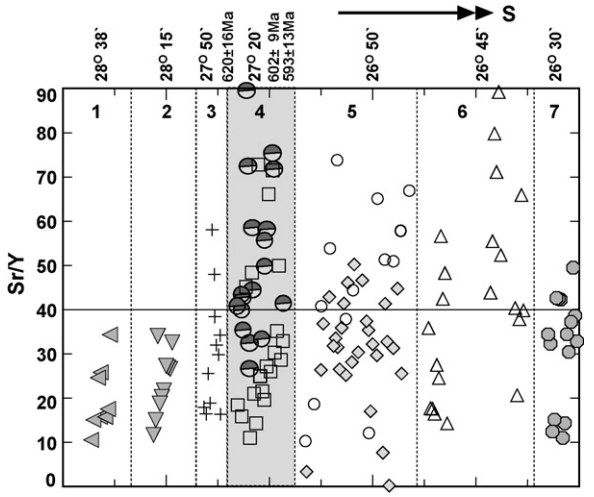

Fig. 11. Latitudinal distribution of Sr/Y in Dokhan Volcanics in the North Eastern Desert. (1) Umm Arta Volcanics (Dawoud, 2000), (2) G. Samr El Qaa (Eliwa, 2000), (3) G. Kharaza (Abdel Rahman, 1996), (4) the studied area (Khalaf, 1999; Present data), (5) Fatira (Ressetar and Monard, 1983; Mohammed et al., 2000), (6) G. Nuqura (Stern and Gottfried, 1986), and (7) S. Safaga (Moghazi, 2003). The numbers (1 and 2) correlate to those in Fig. 1a.

lavas could be the result of partial melting of thick mafic garnetiferous lower continental crust. Recently, the geochemical examination of adakitic lavas suggest that the magma results from the melting of depleted mantle wedge peridotite metasomatized by slab melts or are slab melts that interacted with mantle wedge peridotite (Kay, 1978; Keleman, 1990; Kepezhinskas et al., 1996; Rapp et al., 1999; Smithies and Champion, 2000; Bourdon et al., 2002; Percival et al., 2003; Tatsumi and Hanyu, 2003). Here we examine the origin of the Dokhan adakitic lavas.

5.3.1.1. Are adakitic lavas melts of ANS lower continental crust?. The lower continental crust of the Arabian–Nubian Shield (ANS) has a mafic composition (50 wt.% SiO_2) as inferred from granulite xenoliths (McGuire and Stern, 1993; Mishwat-Al and Nasir, 2004). Stern and Gottfried (1986) suggested melting of the eclogitic lower crust at ~25% or of LREE-enriched garnet peridotite at <10% for the origin of Dokhan Volcanics. Both Dokhan HSA and LSA are enriched in TiO_2, K_2O, P_2O_5, LILE (Rb and Ba), HFSE (Zr and Th), and LREE (Figs. 7 and 8). LSA have SiO_2 contents of basaltic andesite (55 wt.% SiO_2). Although, LREE-enriched feature of the adakites can be generated by melting of eclogitic lower crust at greater pressures (>0.9 GPa garnet stability field; Johannes and Holtz, 1996), it is hard to generate such the mafic composition from melting of the mafic lower crust because of necessary unusually high degree of melting (>40%; Beard and Lofgren, 1991) with unusually high temperature (>1000 °C; Johannes and Holtz, 1996) for the lower crust.

The elevated abundances of compatible elements such as Cr up to 366 ppm, Ni up to 157 ppm, and Mg ($Mg^{\#}$ up to 61) are sometimes greater than those in the crustal rocks and cannot be generated from melting of crustal rocks (Fig. 12a). This is also true for the Dokhan HSA, all of which have greater Ni than those in the ANS lower crustal rocks. If LREE-enriched garnet peridotite (Stern and Gottfried, 1986) was the direct source for the adakites, such the high Cr, Ni, and $Mg^{\#}$ can be achievable. However, melting of peridotite occurs at temperature >1000 °C and the products at <10% melting should be basalts (e.g., Takahashi and Kushiro, 1983). Therefore, garnet peridotite melting is not appropriate for the origin of the Dokhan adakites.

In the study Dokhan lavas, alkali basalt has trace element compositions similar to those of adakites with more elevated Ni, Cr, and $Mg^{\#}$ (Fig. 7). Although this basalt has evidences of a product of peridotite melting with garnet residue, the basalt have similar incompatible element abundance with adakites. It is hard to generate Dokhan adakites by fractional crystallization of the alkali basalt. If it happens, the incompatible element composition of the adakites should be more enriched in contrast to depletion of Ni, Cr, and $Mg^{\#}$ by fractionation of olivine and pyroxenes. However, this is not the case for Dokhan adakites. Therefore, Dokhan adakites cannot be derived from the alkali basalt, which may have originated from mantle peridotite.

Because of the reasons discussed above, we exclude the possibility of the crustal melts for the origin of the Dokhan adakitic lavas.

5.3.1.2. Are adakitic lavas results of slab melt-mantle interaction?. The high compatible element contents (Cr and Ni) of the Dokhan adakites suggest involvement of mantle peridotite. Kamber et al. (2002) argued that Aleutian adakitic arc lavas represent hybrid magmas derived from melting of a subducted eclogitic slab with a small amount of sediments and mantle peridotite. Petrogenetic studies by Samaniego (2001), Bourdon et al. (2002), and Ujike and Goodwin (2002) suggest that partial melts of the subducted oceanic crust interact with mantle peridotite on their way to the surface without significant fractionation or crustal assimilation. Similar interpretations may apply to the Dokhan adakitic lavas.

The Dokhan adakitic lavas plot parallel to the partial melting vector on the La versus La/Yb diagram (Fig. 12b). This geochemical variation cannot be achieved either by fractional crystallization (flat vector) or crustal assimilation because any crustal melts cannot

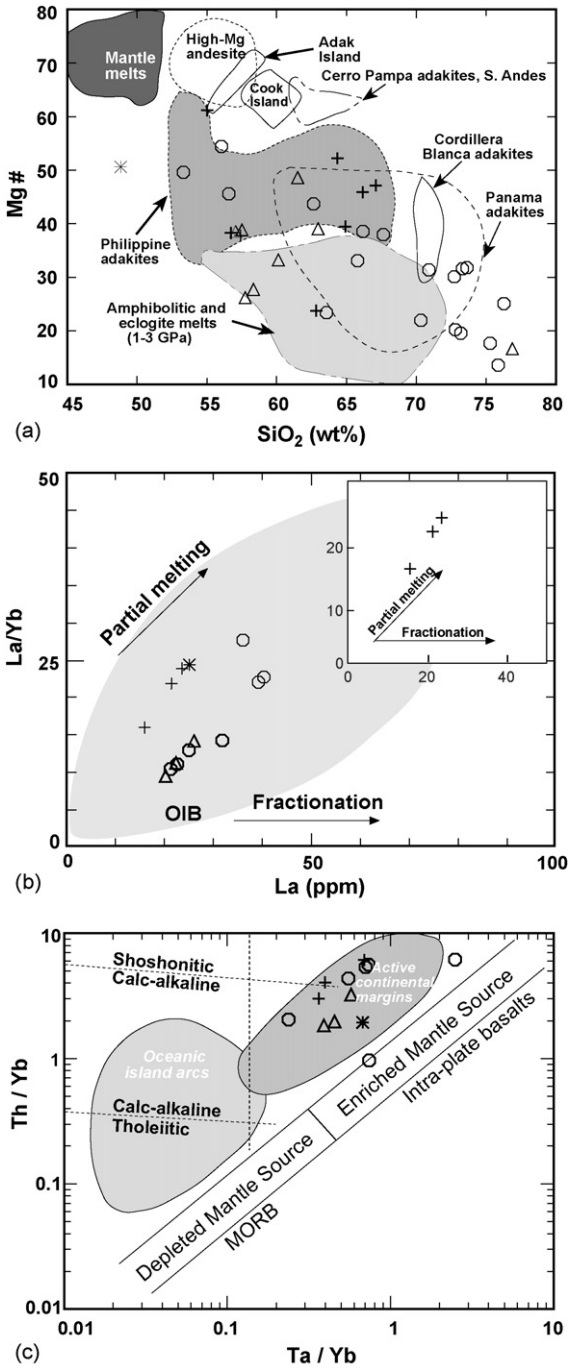

Fig. 12. Bivariant diagrams illustrating the characteristics of Dokhan adakitic lavas: (a) SiO_2 vs. $Mg^{\#}$, (b) La vs. La/Yb, trends are after Kepezhinskas et al. (1997), and (c) Ta/Yb vs. Th/Yb. Comparative adakite fields are from amphibolitic and eclogitic melts and mantle melts (Keleman, 1995). High-Mg andesites (Yogodzinski et al., 1995), mantle-derived adakites of Panama (Defant et al., 1991), Philippines (Sajona et al., 1994), and Cerro Pampa (Kay et al., 1993), crust-derived adakites of Cordillera Blanca (Petford and Atherton, 1996), Adak Island (Kay, 1978), Cook Island (Stern and Kilian, 1996). Symbols as in Fig. 2.

have greater La/Yb than those in adakitic lavas. Interaction between the mantle wedge peridotite and slab melts cannot alter the La/Yb due to low concentration of those elements in the mantle peridotite (Rapp et al., 1999). Instead, if slab melts reacted with mantle peridotite and various amount of garnet is formed in the reaction residue, La/Yb would be changed by the reaction (Rapp et al., 1999). Correlation between La/Yb and $Mg^{\#}$ is observed in Dokhan adakites (Tables 1 and 2) which may indicate the possibility. Therefore, the variable La/Yb can be inherent from the source processes, such as melting degree of subducted oceanic crust or degree of interaction of the slab melt to mantle peridotite. Fractionation of garnet can increase La/Yb. However, garnet is not in liquidus phase of any Dokhan adakites. This possibility is thus negated.

Th/Yb versus Ta/Yb diagram of Pearce (1983) shows that the Dokhan adakitic lavas plot in the field of continental arc together with other calc-alkaline lavas. Adakitic Dokhan lavas tend to plot at higher Th/Yb for a given Ta/Yb compared to the calc-alkaline lavas. In contrast, alkali basalt (US-24) and a high-K calc-alkaline basaltic andesite (US-44) show lower Th/Yb. High Th relative to HREE or LREE is regarded as due to involvement of more subducted sediment (e.g., Plank, 2005) (Fig. 12c). The greater $Mg^{\#}$, Cr, and Ni in Dokhan adakitic lavas is comparable to Philippines adakites, which are thought to have been formed by partial melting of mantle peridotite metasomatized by slab-derived melts (Sajona et al., 1994) (Fig. 12a). The high-$Mg^{\#}$, Cr, and Ni in intermediate Dokhan lavas cannot be achieved by any intra-crustal processes (e.g., Martin et al., 2005 and above discussion) and must be due to reaction with mantle peridotite and felsic slab melts, whichever slab melt later reacted with mantle peridotite (e.g., Samaniego, 2001; Bourdon et al., 2002; Ujike and Goodwin, 2002) or melting of metasomatized mantle by slab melts (Sajona et al., 1994).

Dokhan alkali basalt also has garnet signature (high La_N/Lu_N) and sediment signature (higher Th/Yb) similar to the Dokhan adakitic lavas with low $Mg^{\#}$, Cr, and Ni and high LILEs such as Rb and Ba. These suggest that the source of the alkali basalt and the adakitic lavas would be similar and the apparently common garnet signature comes from melting at high pressure (>2 GPa; Kushiro, 1969). The alkali basalt mantle source would have been metasomatized by slab melts but to lesser extent.

5.3.2. Origin of "common" calc-alkaline lavas

Partial melting of subducted, hydrated oceanic crust modified at 100–200 km depth could generate calc-alkaline magmas of andesitic–dacitic (tonalite) com-

positions (Green and Ringwood, 1968; Green, 1980). However, experimental (Stern, 1974) and geochemical (Gill, 1981) studies concluded that most calc-alkaline andesites are unlikely to be direct partial melts of subducted oceanic crust. The genesis of most typical calc-alkaline arc magmas is generally attributed to melting of mantle peridotite to from basalt as a result of fluxing by small (<2%) amounts of slab-derived melts or fluids (Pearce and Parkinson, 1993), which then fractionates to form andesite and more felsic melts.

The Dokhan basaltic andesite lavas have $SiO_2 \approx 53$ wt.%, $CaO \approx 6$–7.2 wt.%, $Fe_2O_3{}^t \approx 8.1$–10.6 wt.%, and $TiO_2 \approx 1.3$–2.1 wt.% together with the low initial $^{87}Sr/^{86}Sr$ (Stern and Hedge, 1985; Abdel Rahman, 1996) reflecting a mantle peridotite source. The calc-alkaline Dokhan lavas are also similar to present-day calc-alkaline arc lavas; they are enriched in highly incompatible trace elements such as LREE and LILE and not depleted in the HFSE relative to other incompatible elements. However, relatively elevated La_N/Lu_N and Nb–Ta indicate that the Dokhan calc-alkaline lavas belong to continental margin (or rear-arc) environments (see Fig. 12c). These further suggest participation of the subducted oceanic slab melts or fluids for their origin.

5.4. Origin of the Dokhan Volcanics: a ridge subduction model

Coexistence of voluminous calc-alkaline with subordinate adakite and alkali basalt magmas is the key to understanding the origin of Dokhan volcanism. We have discarded the possibility of melting of a thicker ANS lower crust. To generate adakitic lavas for the Dokhan Volcanics, we have proposed the necessity of subducted oceanic slab for the melt source and interaction with mantle peridotite for their elevated $Mg^{\#}$, Cr, and Ni. We also have suggested that slab melt fluxed to the mantle peridotite generated the voluminous calc-alkaline magmas. Existence of alkali magma suggests relatively deep (>60 km; e.g., Kushiro, 1969) asthenospheric mantle source along with the slab-derived magmatism.

In modern arcs, adakite generation has been linked to unusual tectonic settings, such as: (1) Subduction initiation (Sajona et al., 1993; Kimura et al., 2005). (2) Subduction of very young oceanic crust (e.g., Kay et al., 1993). (3) Subduction of plate edges in arc-transform settings (Yogodzinski et al., 2001). (4) Complex sub-arc mantle processes involving multiple stages of metasomatism and melting (Brandon et al., 1999). (5) Post-collisional lithospheric delamination (Saunders et al., 1987; Sajona et al., 2000). Amongst the cases, a similar magma association with Dokhan Volcanics is found in SW Japan (Kimura et al., 2005), where adakite magmas coexist with alkali basalt and calc-alkaline magmas. A similar calc-alkaline to adakitic transition was described by Samaniego et al. (2002) associated with rear-arc alkali basalt activity (Bourdon et al., 2002) from the Northern Volcanic Zone in Ecuador. These two tectonic settings have subduction of Shikoku Basin spreading ridge (Kimura et al., 2005) or the aseismic Carnegie Ridge of the Nazca Plate (Bourdon et al., 2002).

Subduction of spreading ridge or aseismic ridge can cause unusual conditions in the mantle because the hot asthenosphere beneath oceanic slab is dragged down into the subduction zone. Such conditions can generate OIB-type magmas due to deepening of the hot asthenospheric magma source beneath the ridge. Relatively young oceanic crust can also melt to generate adakite magma along with calc-alkaline magmas.

Our tectonic model for the Dokhan Volcanics involves a transition between subduction–collision–post-collision tectonics, previously identified in the region by Beyth et al. (1994). The subduction stage began before ~670 Ma (Stern and Hedge, 1985) and subduction continued as late as ~620 Ma (Stern, 1994). Subduction-related magmatism ceased when terminal collision occurred between East and the West Gondwanaland <630 Ma (e.g., Katz et al., 2004; Miller et al., 2003; Meert, 2003). The Dokhan volcanism took place between ~610 and 560 Ma, after collision in a transitional to extensional tectonic setting (Ressetar and Monard, 1983; Mohammed et al., 2000; Moghazi, 2003). It is possible that oceanic ridges were subducted beneath the region during closure of the Mozambique Ocean, but hot ridges survived beneath suture zone more than 20 Ma after collision. It is supported by the tectonic re-construction of SW Japan arc; the oceanic ridge subducted at 17 Ma stayed beneath the arc at depth 100–150 km over ~17 Ma after subduction and generation of alkali basalts and adakite along with calc-alkaline lavas continued over the time (Kimura et al., 2005). The longevity of the young oceanic plate is perhaps due to buoyant forth of the hot oceanic plate slab.

Such scenario could form hot deep asthenosphere coexisting with oceanic slab, which are requisites for the calc-alkaline–adakite–alkali magma province of the Dokhan Volcanics (Fig. 13). Re-melting of previously metasomatized mantle wedge can explain the origin of the coexisting three lava suites as discussed above; however, heat source (>1000 °C) to generate mantle remelting after collision would require another thermal event. Subduction of hot ocean basin lithosphere is a sort of self-induced mechanism of ocean basin closure and continent-continent collision. We here propose a

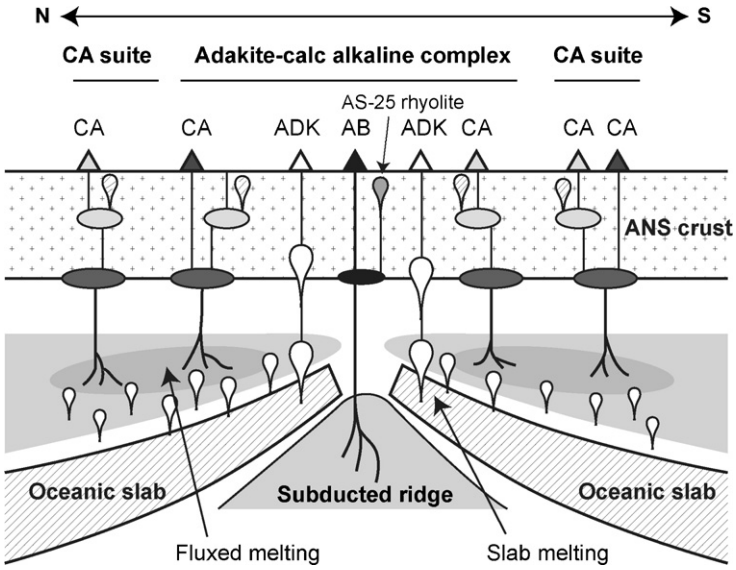

Fig. 13. Cartoon showing NW–SE section beneath the Dokhan Volcanics at ~600 Ma. Perpendicular or oblique subduction of oceanic ridge system would have formed slab melting near the ridge and generated slab melts. The melts erupted immediately after interaction with the mantle to form adakite suite or fluxed mantle peridotite generating calc-alkaline suite magmas. The mantle wedge system is perpendicular to this section allowing NE–SW trending volcanic axis over >200 km for the Dokhan volcanism. Alkali basalt may have been generated as the result of a slab window or by counter flow of mantle asthenosphere induced by subduction. Alkali basalt magma would eventually fractionate to form A_1-type rhyolite. Calc-alkaline suite lavas would have evolved from basalt from melting of the mantle wedge and fractionated to form intermediate to felsic lavas or I-type granitoids. CA: calc-alkaline suite; ADK: adakite suite; AB: alkali basalt suite; ANS: Arabian–Nubian Shield.

ridge (including BAB) subduction during ocean basin closure—slab-melting after continent collision model for the origin of the Dokhan Volcanics. We believe that our scenario best explains the final stage of volcanic activity occurred on the ANS at the end of the Neoproterozoic time.

6. Conclusion

Major and trace elements of basaltic to rhyolitic lavas from the Dokhan Volcanics in Wadi Um Sidra and Wadi Um Asmer areas have been examined. They are predominantly intermediate, medium- to high-K calc-alkaline lavas with subordinate adakitic lavas and minor alkali basalt. Moderate $Mg^{\#}$ and elevated Cr and Ni in adakites suggest that they originated from slab melts that later interacted with mantle peridotite. Calc-alkaline lavas are less fractionated in the HREE than are the adakites with lesser $Mg^{\#}$, Cr, and Ni. Variable LILE and REE contents in the calc-alkaline lavas indicate different degrees of partial melting in the source. Alkali basalt has little Nb–Ta negative anomaly suggesting an OIB mantle source. A ridge subduction model induced by closure of the Mozambique Ocean followed by the Gondwanaland collision best explains the coexistence of the calc-alkaline–adakite–alkali basalt magmas of the Dokhan Volcanics. The volcanism would have induced by remnant hot ridge asthenosphere together with oceanic slab beneath the thick ANS crust due to the burial of the ridge system during the ocean closure event. The Dokhan Volcanics appears to have formed in the transition stage between subduction tectonics and post-collision tectonics induced mainly by the subducted ridge heat source previously existed in oceanic environment.

Acknowledgement

The authors thank Prof. Y. Sawada of Shimane University for free access to the XRF facility. We also greatly thank Prof. R.J. Stern as reviewer for constructive comments on this manuscript.

References

Abdel Rahman, A.M., 1996. Pan-African volcanism: petrology and geochemistry of the Dokhan Volcanic suite in the northern Nubian Shield. Geol. Mag. 133, 17–31.

Abu El Leil, I.A., 1980. Geology, petrography and geochemistry of some granitic rocks in the northern part of the basement complex, Egypt. Unpublished Ph.D. Thesis. Al-Azhar University, Egypt, 294 pp.

Akaad, M.K., Noweir, A.M., 1980. Geology and lithostratigraphy of the Arabian Desert orogenic belt of Egypt between latitudes 25°35′N and 26°30′N. Inst. Appl. Geol. Jeddah Bull. 3, 127–135.

Basta, E.Z., Kotb, H., Awadalla, M.F., 1980. Petrochemical and geochemical characteristics of the Dokhan formation at the type local-

ity, Jabal Dokhan, Eastern Desert, Egypt. Inst. Appl. Geol. Jeddah Bull. 3, 121–140.

Beard, J.S., Lofgren, G.E., 1991. Dehydration melting and watersaturated melting of basaltic and andesitic greenstones and amphibolites at 1, 3 and 6. 9 kb. J. Petrol. 32, 465–501.

Bentor, Y.K., 1985. The crustal evolution of the Arabo-Nubian Massif with special reference to the Sinai Peninsula. Precam. Res. 28, 1–74.

Beyth, M., Stern, R.J., Altherr, R., Kröner, A., 1994. The late Precambrian Timna igneous complex, southern Israel: evidence for comagmatic-type sanukitoid monzodiorite and alkali granite magma. Lithos 31, 103–124.

Brandon, A.D., Becker, H., Carlson, R.W., Shirey, S.B., 1999. Isotopic constraints on time scales and mechanisms of slab material transport in the mantle wedge: evidence from the Simcoe mantle xenoliths, Washington, USA. Chem. Geol. 160, 387–407.

Bourdon, E., Eissen, J.-P., Monzier, M., Robin, C., Martin, H., Cotton, J., Hall, M.L., 2002. Adakite-like lavas from Antisana Volcano (Ecuador): evidence for slab melt metasomatism Beneath the Andean Northern Volcanic Zone. J. Petrol. 43 (2), 199–217.

Calmus, T., Aguillon-Robles, A., Maury, R.C., Bellon, H., Benoit, M., Cotten, J., Bourgois, J., Michaud, F., 2003. Spatial and temporal evolution of basalts and magnesian andesites ("bajaites") from Baja California, Mexico: the role of slab melts. Lithos 66 (1–2), 77–105.

Dawoud, M., 2000. Volcanic arc to transitional environment for the bimodal volcanic suites: an example from the Dokhan Volcanics of Egypt. Sci. J. Fac. Sci. Minufiya Univ. XIV, 47–88.

Defant, M.J., Drummond, M.S., 1990. Derivation of some modern arc magmas by melting of young subducted lithosphere. Nature 347, 662–665.

Defant, M.J., Drummond, M.S., 1993. Mount St. Helens: potential example of the partial melting of the subducted lithosphere in a volcanic arc. Geology 21, 547–550.

Defant, M.J., Richerson, P.M., DeBoer, J.Z., Stewart, R.H., Maury, R.C., Bellon, H., Drummond, M.S., Feigenson, M.D., Jackson, T.E., 1991. Dacite genesis via both slab melting and differentiation: petrogenesis of La Yegueda volcanic complex, Panama. J. Petrol. 32, 1101–1142.

Eby, G.N., 1992. Chemical subdivision of the A-type granitoids: petrogenetic and tectonic implications. Geology 20, 641–644.

El Gaby, S., 1975. Petrochemistry and geochemistry of some granites from Egypt. N. Jb. Miner. Abh. 124, 89–148.

El Gaby, S., List, F.K., Tehrani, R., 1988. Geology, evolution and metallogenesis of the Pan-African belt in Egypt. In: El Gaby, S., Greiling, R.O. (Eds.), The Pan-African Belt of Northeast Africa and Adjacent Areas. Braun, Schweig, Vieweg, pp. 17–68.

El Gaby, S., Khudeir, A.A., El Taky, M., 1989. The Dokhan Volcanics of Wadi Queih area, central Eastern Desert, Egypt. In: Proceedings of the 1st Conference on Geochemistry, Alexandria University, Egypt, pp. 42–62.

El Gaby, S., List, F.K., Tehrani, R., 1990. The basement complex of the Eastern Desert and Sinai. In: Said, R. (Ed.), The Geology of Egypt. Balkema Rotterdam, The Netherlands, pp. 175–184.

Eliwa, H.A., 2000. Petrology, geochemistry, mineral chemistry and petrogenesis of Samr El-Qaa Volcanics, North Eastern Desert, Egypt. Sci. J. Fac. Sci. Minufiya Univ. XIV, 1–45.

El Ramly, M.F., 1972. A new geological map for the basement rocks in the eastern and southwestern deserts of Egypt. Ann. Geol. Surv. Egypt 2, 1–18.

El Sayed, M.M., Obeid, M.A., Furnes, H., Moghazi, A.M., 2004. Late Neoproterozoic volcanism in the southern Eastern Desert, Egypt: petrological, structural and geochemical constraints on the tectonic-magmatic evolution of the Allaqi Dokhan volcanic suite. N. Jb. Miner. Abh. 180 (3), 261–286.

El Shazly, E.M., 1977. The geology of the Egyptian region. In: Narin, A.E., Kanes, W.H., Stehli, F.G. (Eds.), The Ocaen Basins and Margins, Vol. 4A. The Eastern Mediterranean. Plenum Press, New York, pp. 379–444.

Feeley, T.C., Hacker, M.D., 1995. Intracrustal derivation of Na-rich andesitic and dacitic magmas: an example from volcán Ollagüe, Andean Central Volcanic Zone. J. Geol. 103, 213–225.

Fritz, H., Wallbrecher, E., Khudeir, A.A., Abu El Ela, F.F., Dallmeyer, D.R., 1996. Formation of Neoproterozoic metamorphic core complexes during oblique convergence Eastern Desert, Egypt. J. Afr. Earth Sci. 23, 311–329.

Ghanem, M., Dardir, A.A., Francis, M.H., Zalata, A.A., Abu Zeid, K.M., 1973. Basement rocks in eastern Desert of Egypt, north of satitude 26°40′N. Ann. Geol. Surv. Egypt 3, 33–38.

Gill, J., 1981. Orogenic Andesites and Plate Tectonics. Springer, Berlin/Heidelberg/New York, p. 390.

Green, T.H., 1980. Island arc and continent-building magmatism are views of petrogenetic models based on experimental petrology and geochemistry. Tectonophysics 63, 367–385.

Green, T.H., Ringwood, A.E., 1968. Genesis of the calc-alkaline igneous rock suite. Contrib. Miner. Petrol. 18, 105–162.

Greiling, R.O., Abdeen, M.M., Dardir, A.A., El Akhal, H., El Ramly, M.F., Kamal El Din, G.M., Osman, A.F., Rashwan, A.A., Rice, A.H.N., Sadek, M.F., 1994. A structural synthesis of the Proterozoic Arabian–Nubian Shield in Egypt. Geol. Rundsch. 83, 484–501.

Grothaus, B., Eppler, D., Ehrlich, R., 1979. Depositional environments and structural implications of the Hammamat Formation, Egypt. Ann. Geol. Surv. Egypt 9, 564–590.

Hargrove, U.S., Stern, R.J., Kimura, J.-I., Johnson, P., 2004. What is the significance of adakitic granitoids and zircon inheritance in Juvenile arc rocks of the Makkah Batholith, Saudi Arabia? A.G.U. (abstract).

Harms, U., Darbyshire, D.P.F., Denkler, T., Hengst, M., Schandelmeier, H., 1994. Evolution of the Neoproterozoic Delgo suture zone and crustal growth in Northern Sudan: geochemical and radiogenic isotope studies. Geol. Rundsch. 83, 591–603.

Hassan, M.A., Hashad, A.H., 1990. Precambrian of Egypt. In: Said, R. (Ed.), The Geology of Egypts. Alkema, Rotterdam, pp. 201–245.

Hildreth, W., Moorbath, S., 1988. Crustal contribution to arc magmatism in the Andes of Central Chile. Contrib. Miner. Petrol. 98, 455–489.

Irvine, T.N., Barager, W.R.A., 1971. A guide to the chemical classification of the common volcanic rocks, Canada. J. Earth Sci. 8, 523–548.

Jarrar, G., Stern, R.J., Saffarini, G., Al-Zubi, H., 2003. Late- and post-orogenic Neoproterozoic intrusions of Jordan: implications for crustal growth in the northernmost segment of the East African Orogen. Precamb. Res. 123, 295–319.

Johannes, W., Holtz, F., 1996. Petrogenesis and experimental petrology of granitic rocks. Springer-Verlag, Berlin/Heidelberg, p. 333.

Kamber, B.S., Ewart, A., Collerson, K.D., Bruce, M.C., McDonald, G.D., 2002. Fluid-mobile trace element constraints on the role of slab melting and implications for Archaean crustal growth models. Contrib. Miner. Petrol. 144, 38–56.

Kay, R.W., 1978. Aleutian magnesian andesites: melts from subducted Pacific Ocean crust. J. Volcan. Geotherm. Res. 4, 117–132.

Kay, S.M., Ramos, V.A., Marquez, M., 1993. Evidence in Cerro Pampa volcanic rocks for slab-melting prior to ridge trench collision in southern South America. J. Geol. 101, 703–714.

Katz, O., Beyth, M., Miller, N., Stern, R., Avigad, D., Basu, A., Anbar, A., 2004. A Late Neoproterozoic (∼630 Ma) Boninitic Suite from southern Israel: implications for the Consolidation of Gondwanaland. Earth Planet. Sci. Lett. 218, 475–490.

Keleman, P.B., 1990. Reaction between ultramafic rock and fractionated basaltic magma. I. Phase relations, the origin of calc alkaline magma series, and the formation of discordant dunite. J. Petrol. 31, 51–98.

Keleman, P.B., 1995. Genesis of high $Mg^{\#}$ andesites and the continental crust. Contrib. Mineral. Petrol. 120, 1–19.

Kepezhinskas, P., Defant, M.J., Drummond, M.S., 1996. Progressive enrichment of island arc mantle by melt-peridotite interaction inferred from Kamchatka xenoliths. Geochim. Cosmochim. Acta 60, 1217–1229.

Kepezhinskas, P., McDermott, F., Defant, M.J., Hochstaedter, A., Drummond, M.S., Hawkeswaorth, C.J., Koloskov, A., Maury, R.C., Bellon, H., 1997. Trace element and Sr–Nd–Pb isotopic constraints on a three component model of Kamchatka arc petrogenesis. Geochim. Cosmochim. Acta 61, 577–600.

Khalaf, E.A., 1999. Composition-volume changes during metasomatic alteration of Pan-African andesitic volcanic rocks at Gebel El-Dokhan area, northeastern Desert, Egypt. J. King Abdulaziz Univ. Earth Sci. 11, 177–206.

Kimura, J.-I., Yoshida, T., Takaku, Y., 1995. Igneous rock analysis using ICP-MS with internal standardization, isobaric ion overlap correction, and standard addition methods. Sci. Rep. Fukushima Univ. 56, 1–12.

Kimura, J., Yamada, Y., 1996. Evaluation of major and trace elements XRF analyses using a flux to sample ratio of two to one glass beads. J. Min. Petrol. Econ. Geol. 91, 62–72.

Kimura, J.-I., Stern, J.R., Yoshida, T., 2005. Reinitiation of subduction and magmatic responses in SW Japan during Neogene time. Geol. Soc. Am. Bull. 117 (7/8), 969–986.

Kröner, A., Krüger, J., Rashwan, A.A., 1994. Age and tectonic setting of granitoid gneisses in the Eastern Desert of Egypt and south-west Sinai. Geol. Rundsch. 83, 502–513.

Kröner, A., Reischmann, T., Wust, H.-J., Rashwan, A., 1988. Is there any pre-Pan-African (>950 Ma) basement in the Eastern Desert of Egypt? In: El Gaby, S., Greiling, R.O. (Eds.), The Pan-African Belt of Northeast Africa and Adjacent Areas. Vieweg, Braunschweig, pp. 93–119.

Kröner, A., Todt, W., Hussein, I.M., Mansour, M., Rashwan, A., 1992. Dating of late Proterozoic ophiolites in Egypt and the Sudan using single zircon evaporation technique. Precamb. Res. 59, 15–32.

Kushiro, I., 1969. The system forsterite–diopside–silica with and without water at high pressures. Am. J. Sci. Sch. 267-A, 269–294.

Le Maitre, R.W., 1989. A Classification of Igneous Rocks and Glossary of Terms. Blackwell, Oxford, p. 193.

Martin, H., 1987. Petrogenesis of Archaean trondhjemites, tonalites and granodiorites from eastern Finland: major and trace element geochemistry. J. Petrol. 28 (5), 921–953.

Martin, H., 1999. Adakitic magmas: modern analogues of Archean Granitoids. Lithos 26, 411–429.

Martin, H., Moyen, J.-F., 2003. Secular changes in TTG composition: comparison with modern adakites. In: EGS-AGU-EUG Joint Meeting, Nice, April, VGP7-1FR2O-001.

Martin, H., Smithies, R.H., Rapp, R., Moyen, J.-F., Champion, D., 2005. An overview of adakite, tonalite–trondhjemite–granodiorite (TTG), and sanukitoid: relationships and some implications for crustal evolution. Lithos 79, 1–24.

Maury, R.C., Sajona, F.G., Pubellier, M., Bellon, H., Defant, M.J., 1996. Fusion de la croûte océanique dans les zones de subduction/collision récentes: l'exemple de Mindanao (Philippines). Bull. Soc. Geol. Fr. 167 (5), 579–595.

McGuire, A.V., Stern, R.J., 1993. Granulite xenoliths from western Saudi Arabia: the lower crust of the late Precambrian Arabian–Nubian shield. Contrib. Miner. Petrol. 114, 395–408.

Miller, N.R., Alene, M., Sacchi, R., Stern, R., Conti, A., Kröner, A., Zuppi, G., 2003. Significance of the Tambien Group (Tigrai N. Ethiopia) for Snowball Earth Events in the Arabian–Nubian Shield. Precamb. Res. 121, 263–283.

Meert, J.G., 2003. A synopsis of events related to the assembly of eastern Gondwana. Tectonophysics 362, 1–40.

Mishwat-Al, A.T., Nasir, S.J., 2004. Composition of the lower crust of the Arabian Plate: a xenolith perspective. Lithos 72, 45–72.

Moghazi, A.M., 1994. Geochemical and radiogenic isotope studies of some basement rocks at the Kid area, southeastern Sinai, Egypt. Unpublished Ph.D. Thesis. Alexandria University, Egypt, 377 pp.

Moghazi, A.M., 2003. Geochemistry and petrogenesis of a high-K calc-alkaline Dokhan Volcanic suite, South Safaga area, Egypt: the role of late Neoproterozoic crustal extension. Precamb. Res. 125, 161–178.

Moghazi, A.M., Mohamed, F.H., Kanisawa, S., 1999. Geochemistry and petrogenesis of late Proterozoic plutonic rock suites in the Homrit Waggat and El Yatima areas, Eastern Egypt. J. Afr. Earth Sci. 29, 535–549.

Mohamed, F.H., Hassanen, M.A., Matheis, G., Shalaby, M.H., 1994. Geochemistry of the Wadi Hawashia granite complex. northern Egyptian Shield. J. Afr. Earth Sci. 19, 61–74.

Mohammed, F.H., Moghazi, A.M., Hassanen, M.A., 2000. Geochemistry, petrogenesis and tectonic setting of late Neoproterozoic Dokhan-type volcanic rocks in the Fatira area, eastern Egypt. Inter. J. Earth Sci. 88, 764–777.

Pearce, J.A., 1983. Role of the sub-continental lithosphere in magma genesis at active continental margins. In: Hawkesworth, C.J., Norry, M.J. (Eds.), Continental Basalts and Mantle Xenoliths. Shiva Publishing Limited, pp. 230–249.

Pearce, J.A., Gorman, B.E., Birkett, T.C., 1975. The TiO_2–K_2O–P_2O_5 diagram: a method of discriminating between oceanic and non-oceanic basalts. Earth Planet. Sci. Lett. 24, 419–426.

Pearce, J.A., Gale, G.H., 1977. Identification of ore-depositional environment from trace-element geochemistry of associated igneous host rocks. In: Volcanic Processes in Ore Genesis, vol. 7. Special Pub. Geol. Soc., London, pp. 14–24.

Pearce, J.A., Cann, J.R., 1973. Tectonic setting of basic volcanic rocks determined using trace element analyses. Earth Planet. Sci. Lett. 19, 290–300.

Pearce, J.A., Harris, N.B.W., Tindle, A.G., 1984. Trace element discrimination diagrams for the tectonic interpretation of granitic rocks. J. Petrol. 25 (4), 956–983.

Pearce, J.A., Parkinson, I.J., 1993. Trace element models for mantle melting: approach to volcanic arc petrogenesis. In: Pritchard, H.M., Alabaster, T., Harris, N.B.W., Neary, C.R. (Eds.), Magmatic Processes and Plate Tectonics, vol. 76. Special Pub. Geol. Soc., London, pp. 373–403.

Percival, J.A., Stern, R.A., Rayner, N., 2003. Archean adakites from the Ashuanipi complex, eastern Superior Province, Canada: geochemistry, geochronology and tectonic significance. Contrib. Miner. Petrol. 145, 265–280.

Petford, N., Atherton, M.P., 1996. Na-rich partial melts from newly underplated basaltic crust: the Cordillera Blanca Batholith. Peru. J. Petrol. 37, 1491–1521.

Plank, T., 2005. Constraints from thorium/lanthanum on sediment recycling at subduction zones and the evolution of the continents. J. Petrol. 46, 921–944.

Rapp, R.P., Shimizu, N., Norman, M.D., Applegate, G.S., 1999. Reaction between slab-derived melts and peridotite in the mantle wedge: experimental constraints at 3.8 GPa. Chem. Geol. 160, 335–356.

Ressetar, R., Monard, J.R., 1983. Chemical composition and tectonic setting of the Dokhan Volcanic formation, Eastern Desert, Egypt. J. Afr. Earth Sci. 1, 103–112.

Ries, A.C., Shackelton, R.M., Graham, R.H., Fitches, W.R., 1983. Pan-African structures, ophiolites and melange in the Eastern Desert of Egypt: a traverse at 26°N. J. Geol. Soc. Lond. 140, 75–95.

Rogers, G., Saunders, A.D., Terrell, D.J., Verma, S.P., Marriner, G.F., 1985. Geochemistry of Holocene volcanic rocks associated with ridge subduction in Baja California, Mexico. Nature 315, 389–392.

Roser, B.P., Kimura, J.-I., Hisatomi, K., 2000. Whole-Rock Elemental Abundances in Sandstones and Mudrocks from the Tanabe Group, Kii Peninsula, Japan, vol. 19. Sci. Report Dept. Geosci., Shimane Univ., pp. 101–112.

Sajona, F.G., Maury, R.C., Bellon, H., Cotton, J., Defant, M.J., Pubellier, M., 1993. Initiation of subduction and the generation of slab melts in western and eastern Mindanao, Philippines. Geology 21, 1007–1010.

Sajona, F.G., Maury, R.C., Pubellier, M., Leterrier, J., Bellon, H., Cotton, J., 2000. Magmatic source enrichment by slab-derived melts in a young post-collisional setting, central Mindanao (Philippines). Lithos 54, 173–206.

Sajona, F.G., Bellon, H., Maury, R.C., Pubellier, M., Cotton, J., Rangin, C., 1994. Magmatic response to abrupt changes in geodynamic settings: Pliocene-Quaternary calc-alkaline and Nb enriched lavas from Mindanao (Philippines). Tectonophysics 237, 47–72.

Samaniego, P., Martin, H., Robin, C., Monzier, M., 2002. Transition from calc–alkalic to adakitic magmatism at Cayambe volcano, Ecuador: insights into slab melts and mantle wedge interactions. Geology 30 (11), 967–970.

Samaniego, P., 2001. Transition entre magmatismes calco-alcalin et adakitique dans le cas d'une subduction impliquant une ride ocèanique: Le volcan Cayambe (Equater). Ph.D. Thesis. Universitè Blaise Pascal, Clermont-Ferrand.

Saunders, A.D., Rogers, G., Marriner, C.F., Terrell, D.J., Verma, S.P., 1987. Geochemistry of Cenozoic volcanic rocks, Baja California, Mexico: implications for the petrogenesis of post-subduction magmas. J. Volcan. Geotherm. Res. 32, 223–245.

Schandelmeier, H., Richter, A., Harms, U., 1987. Proterozoic deformation of the East Saharan Craton in southeast Libya, south Egypt, and north Sudan. Tectonophysics 140, 233–246.

Smithies, R.A., 2000. The Archaean tonalite-trondhjemite-granodiorite (TTG) series is not an analogue of Cenozoic adakite. Earth Planet. Sci. Lett. 182, 115–125.

Smithies, R.A., Champion, D.C., 2000. The Archean high-Mg diorite suite: links to tonalite-trondhjemite- granodiorite magmatism and implications for early Archaean crustal growth. J. Petrol. 41, 1653–1671.

Stern, C.R., 1974. Melting products of olivine tholeiite basalt in subduction zones. Geology 2, 227–230.

Stern, C.R., Kilian, R., 1996. Role of the subducted slab, mantle wedge and continental crust in the generation of adakites from the Andean Austral Volcanic Zone. Contrib. Miner. Petrol. 123, 263–281.

Stern, R.J., 1979. Late Precambrian ensimatic volcanism in the central Eastern Desert of Egypt. Ph.D. Thesis. San Diego, California University, 210 pp.

Stern, R.J., 1981. Petrogenesis and tectonic setting of Late Precambrian ensimatic volcanic rocks, central Eastern Desert of Egypt. Precamb. Res. 16, 195–230.

Stern, R.J., 1994. Arc assembly and continental collision in the Neoproterozoic East African Orogen: implications for the consolidation of Gondwanaland. Ann. Rev. Earth Planet. Sci. 22, 319–351.

Stern, R.J., 2002. Crustal evolution in the east African Orogen: a neodymium isotope prospective. J. Afr. Earth Sci. 34, 109–117.

Stern, R.J., Gottfried, D., 1986. Petrogenesis of late Precambrian (575–600 Ma) bimodal suite in northeast Africa. Contrib. Miner. Petrol. 92, 492–501.

Stern, R.J., Gottfried, D., Hedge, C.E., 1984. Late Precambrian rifting and crustal evolution in the northeast Desert of Egypt. Geology 12, 168–172.

Stern, R.J., Hedge, C.E., 1985. Geochronologic and isotopic constraints on late Precambrian crustal evolution in the Eastern Desert of Egypt. Am. J. Sci. 285, 97–127.

Stern, R.J., Sellers, G., Gottfried, D., 1988. Bimodal dyke swarms in the North Eastern Desert of Egypt: significance for the origin of late Precambrian "A-type" granites in northern Afro-Arabia. In: El Gaby, S., Greiling, R.O. (Eds.), The Pan-African Belt of Northeast Africa and Adjacent Areas. Vieweg, Weisbaden, pp. 147–177.

Sultan, M., Tucker, R.D., El Alfy, Z., Attia, R., Ragab, A.G., 1994. U–Pb (zircon) ages for the gneissic terrane west of the Nile, southern Egypt. Geol. Rundsch. 83, 514–522.

Takahashi, E., Kushiro, I., 1983. Melting of a dry peridotite at high pressures and basalt magma genesis. Am. Miner. 68, 859–879.

Tatsumi, Y., Hanyu, T., 2003. Geochemical modeling of dehydration and partial melting of subducting lithosphere: toward a comprehensive understanding of high-Mg andesite formation in the Setouchi volcanic belt, SW Japan. Geochem. Geophys. Geosyst. 4 (9), 1081, doi:10.1029/2003GC000530.

Ujike, O., Goodwin, A.M., 2002. Geochemistry of shoshonites from the Upper Keewatin Assemblage, western Wabigoon Belt, Superior Province, Canada. J. Miner. Petrol. Sci. 97, 269–277.

Vail, J.R., 1985. Pan-African (Late Precambrian) tectonic terrains and the reconstruction of the Arabian–Nubian Shield. Geology 13, 839–842.

Whalen, J.B., Currie, K.L., Chappell, B.W., 1987. A-type granites: geochemical characteristics, discrimination and petrogenesis. Contrib. Mineral. Petrol. 95, 407–419.

Whalen, J.B., Percival, J.A., McNicoll, V.J., Longstaffe, F.J., 2002. A mainly crustal origin for tonalitic granitoid rocks, Superior Province, Canada: implications for late Archean tectonomagmatic processes. J. Petrol. 43, 1551–1570.

Wilde, S.A., Yossef, K., 2000. Significance of SHRIMP U–Pb dating of the Imperial Porphyry and associated Dokhan Volcanics, Gebel Dokhan, North Eastern Desert, Egypt. J. Afr. Earth Sci. 31, 403–413.

Willis, K.M., Stern, R.J., Clauer, N., 1988. Age and geochemistry of late Precambrian sediments of the Hammamat Series from the northeastern Desert of Egypt. Precamb. Res. 42, 173–187.

Yogodzinski, G.M., Kay, R.W., Volynets, O.N., Loloskov, A.V., Kay, S.M., 1995. Magnesian andesite in the western Aleutian Komandorsky region: implications for slab melting and processes in the mantle wedge. Geol. Soc. Am. Bull. 107, 505–519.

Yogodzinski, G.M., Lees, J.M., Churikova, T.G., Dorendorf, F., Woerner, G., Volynets, O.N., 2001. Geochemical evidence for the melting of subducting oceanic lithosphere at plate edges. Nature 409, 500–504.